# Evaluating impact and recovery of mangroves following extreme climatic events using satellite remote sensing in Exmouth Gulf, north western Australia

**Zoe Stewart-Yates**

Supervisors: Dr Halina Kobryn & Dr Margaret Andrew

## Declaration

I, Zoe Stewart-Yates, declare that this is wholly my own research and that any other research has been duly cited.

## Abstract

The objective of this study was to study mangrove response (impact and recovery) from extreme climatic events such as tropical cyclones, marine heatwaves, and drought events on the eastern shores of Exmouth Gulf. Mangroves in arid regions, like those in Exmouth, are considered the most sensitive to disturbances due to already existing at their physiological limits. Projected increase in frequency, severity and duration of climate extremes is also considered a major challenge for mangroves in the future. Mangroves are critically important communities providing a wide variety of essential ecosystem services and coastal protection, making it important to monitor them from these events and assess recovery.

This study used satellite remote sensing and a multiple endmember spectral mixture analysis (MESMA) to detect and quantify impact and track recovery of mangroves from 1998 to 2021. This study found that greater impacts on mangroves were associated with cyclone and drought events, whereas marine heatwaves did not cause much impact. It was also demonstrated that cyclones tended to result in increases in mangrove cover. A cyclone associated with rainfall occurring before a drought event may have ameliorated extreme drought conditions, potentially reducing the disturbance of this event on mangroves. In addition, recovery from one cyclone was particularly slow, however this may be attributed to an extreme drought event that occurred four years later which also resulted in high impact and slow recovery. This raises the concern of compound impacts slowing recovery of mangroves in the area. Impacts associated with one marine heatwave, considered due to other causes, which resulted in lower magnitudes of negative impact resulted in more rapid mangrove recovery.

This study has found additional impacts on mangroves in Exmouth Gulf that had previously gone unreported, demonstrating the importance of remote sensing in monitoring these communities. In addition, demonstrating the need for further long-term monitoring of these mangroves.

## Acknowledgements

I would like to extend my deepest gratitude to my supervisors, Dr Halina Kobryn and Dr Margaret Andrew, for being great mentors over this past year and always being available for support. A special thanks to my mum, Dr Amanda Yates, who has been willing to read drafts, be an ear to discuss my research with and a major rock of support throughout the duration of all my studies but especially this one. I would also like to acknowledge my family, especially my brother, and my partner who have also helped with aspects of this project and provided further encouragement and additional support.

# Table of Contents

**Declaration** ..... ii
**Abstract** ..... ii
**Acknowledgements** ..... iii
**1.0 Introduction** ..... 1
1.1 Arid zone mangroves ..... 1
1.2 Climatic disturbance and recovery ecology of mangroves ..... 1
1.3 Monitoring mangroves ..... 4
1.4 The regional setting of Exmouth Gulf ..... 4
1.5 Research aims ..... 6
2.0 Methods ..... 8
2.1 Study area ..... 8
2.2 Climatic events ..... 10
2.3 Data and pre-processing ..... 13
2.3.1 Climate data ..... 13
2.3.2 Remote sensing data and selection criteria ..... 14
2.4 Multiple Endmember Spectral Mixing Analysis (MESMA) ..... 16
2.4.1 Endmember selection ..... 18
2.4.2 Optimisation of endmembers ..... 19
2.4.3 Application of MESMA ..... 22
2.5 Change analysis ..... 24
2.5.1 Impact detection and quantification ..... 24
2.5.2 Recovery ..... 24
**3.0 Results** ..... 27
3.1 Impacts ..... 27
3.2.1 Whole study area impacts ..... 27
3.1.2 Impacts across regions of the study area ..... 30
3.1.3 Impacts across different distances from the coastline ..... 35
3.2 Recovery ..... 38
**4.0 Discussion** ..... 50
4.1 Mangrove response to climatic impacts ..... 50
4.2 Mangrove recovery from impacts ..... 53
4.3 Limitations and future study ..... 54
**5.0 Conclusions** ..... 55
**6.0 References** ..... 57
**Appendix A** ..... 65
**Appendix B** ..... 67

# 1.0 Introduction

## 1.1 Arid zone mangroves

Mangroves are globally important intertidal halophytes that provide a wide variety of ecosystem services and coastal protection (Barbier et al., 2011). They are, however, declining globally due to natural and anthropogenic disturbances (Goldberg et al., 2020). Arid zone mangroves are arguably the most sensitive mangrove communities to disturbances due to already existing at the edge of their physiological limits (Adame et al., 2021). Because mangroves in arid climate zones have adapted to challenging environmental conditions such as hypersaline mudflats, variable and infrequent precipitation and low nutrients, they are fundamentally different from tropical assemblages (Adame et al., 2021).

Because arid zone mangroves occur at their tolerance thresholds, they have lower productivity and growth, and shorter stands than tropical conspecifics (Adame et al., 2021). Low growth and low diversity in these regions have been attributed to limited nitrogen and low precipitation, respectively, with few species able to tolerate and maintain productivity under hypersaline soils (i.e. due to poor flushing), low nutrients and low humidity (Ball & Farquhar, 1984; Osland et al., 2017; Adame et al., 2021). Despite the lower productivity, they present disproportionately high ecosystem services for their region because they are one of the few woody communities that can grow in hot, arid and saline environments (Adame et al., 2021). They also provide large carbon sequestration and store more carbon belowground than tropical mangrove forests and terrestrial forests (Lugo, 1997; Lovelock, 2008). This is potentially linked to the amount of below ground and soil carbon stores needed to withstand unfavourable environmental conditions such as low nutrient availability and anaerobic conditions typical for arid zone regions (Lovelock, 2008).

## 1.2 Climatic disturbance and recovery ecology of mangroves

Mangroves have managed to survive various extreme climatic events over several millennia (Alongi, 2015). However, concerns of future mangrove survival are arising from scientists because of rapid anthropogenic climate change (Asbridge et al., 2015; Harris et al., 2018; Sippo et al., 2018). This concern stems from projected increases in severity and frequency of extreme climatic events due to climate change, which have already been increasing in

severity, frequency and extent during recent decades (Bergstrom et al., 2021). Climate extreme events and their associated impacts may be most damaging to mangroves with projected increased frequencies likely to drive an ecosystem collapse (Babcock et al., 2019). With increasing frequency of disturbances there is concern mangroves may not be able to recover quickly enough, where time between successive disturbances may not be sufficient for full recovery (Asbridge et al., 2015; Harris et al., 2018).

Mangroves are known to be strongly influenced by atmospheric temperature, mean sea level, salinity and extreme events in relation to precipitation (e.g. drought and flooding) (Asbridge et al., 2015; Lovelock et al., 2017). Climatic events can influence these factors and exacerbate the environmental stressors of mangroves. Drought conditions and events are expected to be more frequent with climate change, leading to higher salinities which may exceed salinity tolerances of mangroves more often (Alongi, 2015). Tropical cyclones have a range of effects both negative and positive, which may depend on the mangroves' position relative to the storm track or the severity of weather associated with the cyclone. Destructive tropical cyclones (most likely passing over mangroves) bearing strong winds can cause defoliation or completely uproot the mangroves (Asbridge et al., 2015). Arid zone mangroves may be initially less affected by lower category cyclones due to their short stature, making them more wind resilient (Roth, 1992; Krauss & Osland, 2020). Additionally, high rainfall associated with tropical cyclones can flood mangroves and disturb sediment accretion and storm surges can cause sediment deposition (Paling et al., 2008; Asbridge et al., 2015; Sippo et al., 2018). Conversely, cyclones that are rain-bearing (passing nearby) can provide essential water input which alleviates mangroves from dry hypersaline conditions and allow for nutrient flow to promote growth (Lovelock et al., 2011). Depending on the severity of the impact and the responses of different mangrove species these climatic events can lead to changes in growth productivity, canopy structure and species composition, landward and seaward expansion, and geographical distribution (Duke, 1990; Asbridge et al., 2015; Lovelock et al., 2017).

Cumulative impacts may become more likely under climate change, with increased risk of successive extreme climatic events, which may have implications for mangrove recovery. Continued disturbance due to regular extreme climatic events can prevent recovery of mangroves to previous community extent affecting long-term survival (Harris et al., 2018). Further periods or events of drought following extreme events can limit mangrove recovery

and potentially lead to further degradation (Dai, 2013; Duke et al., 2017; Servino et al., 2018). Although lower growth heights could be advantageous in limiting wind effects, lower growth potential of mangroves in arid zone climates could result in slow recovery (Roth, 1992; Krauss & Osland, 2020). Mangrove communities that are spatially extensive are considered to be more resilient to climatic events due to having a higher likelihood of having surviving areas that can serve as seed and propagule sources for impacted areas which can facilitate recovery (Harris et al., 2018; Krauss & Osland, 2020). Weather effects associated again from tropical cyclones may provide opportunity for mangrove recovery. Inundation by storm surges and high tides may protect seedings, saplings and small mangrove stands from high winds during cyclones, leaving areas potentially unaffected (Stocker, 1976; Paling et al., 2008; Krauss & Osland, 2020).

Extreme climatic events have caused some of the largest mortality and dieback events of mangroves in the world, they are the largest contributor of mangrove decline in Australia with negative impacts being most notable in northwest Australia (Giri et al., 2011; Goldberg et al., 2020). Additionally, half of the reported losses of mangroves, in Australia, due to natural impacts have been caused by tropical cyclones (Sippo et al., 2018). The majority of mangrove mortality attributed to tropical cyclones in the southern hemisphere has been in Australia, however this could be due to greater research effort in Australia (Sippo et al., 2018). Other reported impacts from natural events in Australia have been associated with the El Niño Southern Oscillation (ENSO), especially the El Niño phase. Mangrove mortality events associated with El Niño phases have been attributed to low rainfall, record high atmospheric temperatures and low sea level, leading to drought conditions (Duke et al., 2017; Lovelock et al., 2017; Hickey et al., 2021). In Australia, mangrove mortality that has been associated with drought conditions have been predominantly linked to the El Niño phase of ENSO, with multiple recent accounts of mangrove decline following these drought events (Lovelock et al, 2017; Duke et al., 2017; Sippo et al., 2018; Asbridge et al., 2019; Hickey et al., 2021). Potential impacts due to marine heatwaves (MHW) or other modes of climate variability (e.g. La Niña) have not been equally explored (but see Duke et al., 2017; Hickey et al., 2021).

## 1.3 Monitoring mangroves

Remote sensing methods have provided great opportunity to monitor mangrove ecosystems at the landscape scale. Mangroves tend to cover large areas and are often impracticable for field research (Pham et al., 2019). Furthermore, arid zone mangroves are typically in remote regions that are largely inaccessible (Adame et al., 2021). Remote sensing techniques have been particularly useful for change detection studies utilising time series data to monitor mangrove ecosystems at large scale, including changes associated with climatic disturbance events (Paling et al., 2008; Duke et al., 2017; Lovelock et al., 2017; Asbridge et al., 2019; Servino et al., 2018; Goldberg et al., 2020; de Jong et al., 2021). Satellite data archives can allow researchers to go back in time and investigate climate impacts that previously received little study. Mangroves are also quite recognisable when using remotely sensed data due to a distinct spectral signature, with low spectral reflectance (absorbance) in the red and relatively high spectral reflectance in the near-infrared wavelengths (Giri, 2016; de Jong et al., 2021). This makes them distinguishable from other coastal land cover types within these systems such as mud flats, saltmarshes and algal mats (de Jong et al., 2021).

## 1.4 The regional setting of Exmouth Gulf

Climate drivers on northwest of Australia differ from those in other parts of the world. The dominant mode of climate variability in this region is the Ningaloo Niño/Niña which is driven by broader scale influences such as the Australian summer monsoon and ENSO (Feng et al., 2013; Kataoka et al., 2014; Zhang et al., 2018; Kataoka et al., 2018; Maggiorano et al., 2021). The Ningaloo Niño is associated with positive (warm) sea surface temperature (SST) anomalies and Ningaloo Niña with negative (cold) SST anomalies, with both generally peaking in the austral summer (Kataoka et al., 2014). The Ningaloo Niño is a major cause of marine heatwaves (MHW) for this region where local coupled atmosphere–ocean feedback amplifies positive (warm) SST resulting in a MHW (Kataoka et al. 2014; Marshall et al., 2015; Hobday et al., 2016; Zhang et al., 2018; Maggiorano et al., 2021).

La Niña phases have previously been identified as the major cause of Ningaloo Niño generating MHWs, however MHWs have occurred during El Niño phases and independent of ENSO (e.g. caused by the Australian Summer Monsoon) (Kataoka et al., 2014, 2018;

Maggiorano et al., 2021). In addition to contributing to the formation of the Ningaloo Niño/Niña and consequently MHWs, the broader scale ENSO cycle can have local effects, especially on sea level. During El Niño phases, sea levels tend to be lower (negative anomalies) and during La Niña, sea levels tend to be higher (positive anomalies) (Merrifield et al., 2012; Deepa et al., 2019). Low sea level caused by this phase, in addition to other variables such as low or no precipitation influenced by other modes in north west Australia, can lead to drought conditions due to less tidal flushing leading to higher salinities. Although explored elsewhere in Australia (Duke et al., 2017; Lovelock et al., 2017; Asbridge 2019), the effect of MHWs and El Niño's on mangroves have not been investigated in Exmouth Gulf.

This region has historically been vulnerable to tropical cyclones and tsunamis with mangroves here occurring within the most cyclone-prone region across the entire Australian coastline (McBride, 2012; May et al., 2015) (See Figure 1.1). In addition, the La Niña phase of ENSO that generates MHWs can result in greater occurrences of tropical cyclones in this region (Kuleshov et al., 2008). During a recent preliminary assessment, increased climatic impacts due to climate change have been considered high risk to mangroves in Exmouth Gulf (Sutton & Shaw, 2021). This makes monitoring of this ecosystem crucial, given that climatic impacts are already a natural feature that may become more frequent and severe. Although mangroves in Exmouth Gulf have received little attention following ENSO and MHW events, a study has been conducted in this region for a particularly strong Tropical Cyclone that caused significant mortality in 1999 (Cyclone Vance) (See Paling et al., 2008), however the mangroves were still recovering at the time of the study and thus it is still uncertain if mangroves in Exmouth Gulf have since recovered.

Evaluating mangrove response to climatic events in this region is critical as these mangroves play significant ecological and economic roles, forming an important part of the ecosystem. Mangroves here provide essential habitat for the juvenile stages of reef organisms associated with the world heritage listed Ningaloo Reef and a variety of invertebrate species including endemic crab species (Humphreys et al., 2005; Wilson, 2013). Mangrove canopy size or extent may also contribute to fishery stocks where reduced mangrove area may negatively impact fishery sizes (Loneragan et al., 2005). Further, the proximity of seagrass to mangroves enhances the habitat capabilities of seagrass for fisheries through added provisions of food and shelter (Nagelkerken et al., 2001; Skilleter et al., 2005; Unsworth et al., 2008).

## 1.5 Research aims

The mangroves in Exmouth Gulf have remained relatively undisturbed from anthropogenic disturbances since around 1972 when a salt production development was abandoned (Gulf Holdings, 1990). Exmouth Gulf mangroves have been recognised as regionally and nationally important, where their protection and conservation are supported under a number of State and Federal Acts, thus warranting high protection from anthropogenic disturbances (Lane et al., 2001; Humphreys et al., 2005; EPA, 2009; Sutton & Shaw, 2021). Thus, in this region, the major threats to mangroves are climatic impacts. Identifying how differing climatic events impact mangroves and how quickly mangroves can recover from climatic disturbances may provide valuable understanding for mangrove protection into the future, and consequently support habitat protection for a variety of other biota that rely on mangroves.

The aim of this study is to provide a recent evaluation of mangrove response to a variety of climatic disturbances. This study will use satellite remote sensing to detect and quantify impacts from extreme climatic events that occurred on the eastern Exmouth Gulf between 1999 and 2016, including from tropical cyclones, strong ENSO phases causing drought events and marine heatwaves generated by varying climate modes, and track mangrove recovery from these climatic events from 1998 to 2021.

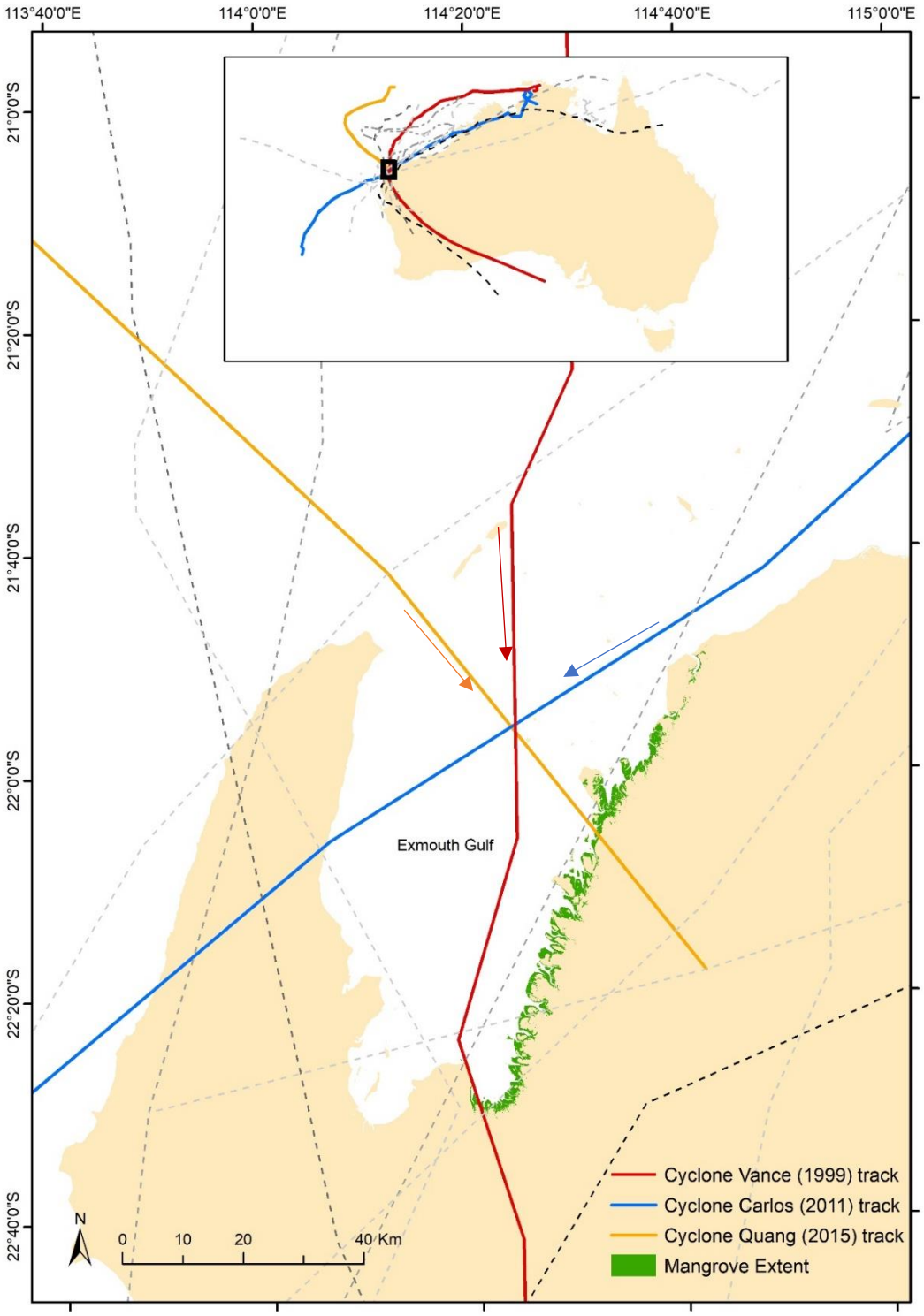


**Figure 1.1:** Historical geographical tracks of tropical cyclones that have passed nearby and over the Exmouth Gulf from 1970 – 2017. The line style and tone of cyclone tracks indicate the time frames in which cyclones occurred, showing cyclones from the 1970s (light grey dotted line), 1980s (medium grey dotted line), 1990s (dark grey dotted line), 2000s (black dotted line) and 2010s (orange and blue lines). Cyclone tracks in solid-coloured lines indicate the most recent cyclones to pass directly through the gulf, Tropical Cyclone Vance 1999 (red line), Carlos 2011 (blue line) and Quang 2015 (orange line), where respective coloured arrows indicate direction of cyclone track, these are the cyclones that are included in this study.

# 2.0 Methods

## 2.1 Study area

Exmouth Gulf is a 2900 $km^2$ U-shape embayment situated 22°11'S, 114°33'E on the northwest shelf of Western Australia (Figure 2.1). It is characterised by a shallow basin (≤ 22m depth), limestone shores on the western and southern coasts as remnants from fringing coral reefs during the late Pleistocene Epoch (Wilson, 2013), and extensive mangrove habitat on the eastern shore which is the focus of this study (Figure 2.1). The mangroves cover an area of ~377 $km^2$, along ~82 km of coastline (calculated with GIS software).

This region has an arid climate with mild winters and hot summers. It occurs along the most arid zone across the entire Australian coastline (Semeniuk, 1996). Average monthly maximum atmospheric temperatures range between 24 °C for winter and 38 °C for summer, with the lowest and highest daily maximum temperatures recorded at 21 °C (winter) and 41 °C (summer) (BOM, 2021). Average monthly Sea Surface Temperature (SST) ranges from 19 °C to 31 °C with the minimum and maximum daily SST recorded being 17 °C and 32 °C (NASA, 2021). This region experiences semi-diurnal tides of about 2 meters. The majority of rainfall (~ 240mm $year^{-1}$) occurs during winter months (May and June) and during cyclone season (January to March) when there is an active tropical cyclone or tropical low (BOM, 2021).

From northern Australia southwest to the Exmouth Gulf mangrove species richness decreases as the coast becomes more arid, to more specialised species (Semeniuk, 1996; Wilson, 2013). The eastern Exmouth Gulf hosts a few species of mangrove able to tolerate this type of climate including mainly *Avicennia marina.* Mangroves within the genus *Avicennia* are markedly versatile species occurring across diverse climate zones, with species exhibiting freeze tolerance (e.g. *Avicennia germinans*) and considerable salt tolerance (e.g. *Avicennia marina*) (Osland et al., 2016; Humphreys et al., 2005). *Avicennia* species often dominate mangroves in arid climates (Adame et al., 2021). The second most abundant species in Exmouth Gulf is *Rizophora stylosa,* and the less common species include *Ceriops tagal*, *Ceriops australis*, *Aegialitis annulate* and *Bruguiera exaristata* (Humphreys et al., 2005).

A study area mask was used as part of this study, encompassing a 5 km distance from shore buffer to ensure entire creeks were captured and areas likely to experience tidal fluctuation

including from climatic events using a water observation from space layer (Geoscience Australia, 2004; https://nationalmap.gov.au/).

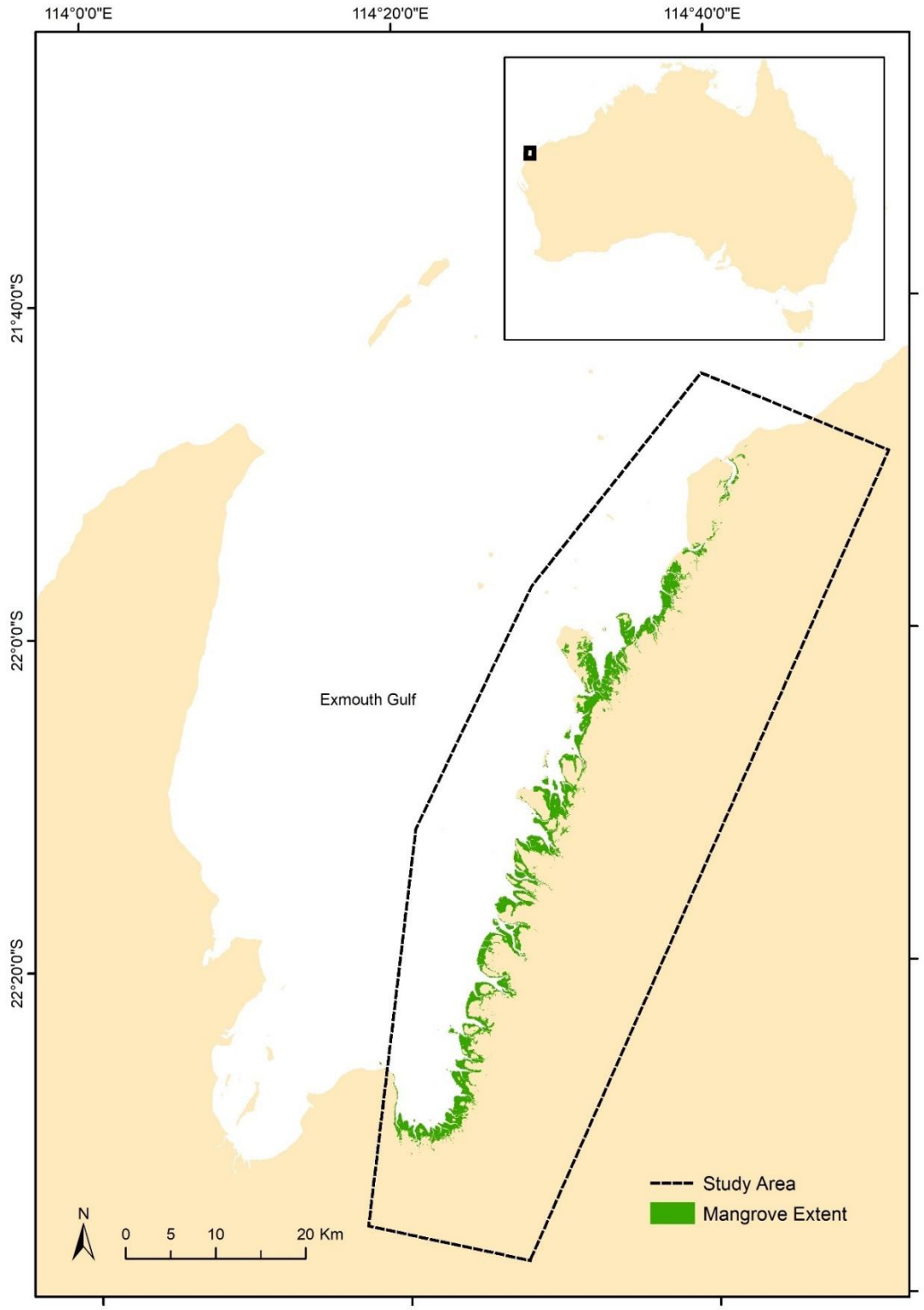


**Figure 2.1:** Study area of eastern Exmouth Gulf (black dashed line), and the extent of mangroves along this coast in addition to its region of Australia.

## 2.2 Climatic events

This study will evaluate the responses (impacts and recovery) of mangroves to extreme climatic impacts including three tropical cyclones, two drought events (El Niño phases) and two MHWs both generated by different means (Table 2.1). All of these climatic events occurred during a particular climate mode, most notably with ENSO phases, with the co-occurring events mostly associated with these broader climate modes. For example, Cyclone Carlos occurred after the peak of Ningaloo Niño 10-11 (occurring with La Niña) and Cyclone Quang before the peak Ningaloo Niña 15-16 (8 months prior) (occurring with El Niño) and thus might be considered as having cumulative impact (Table 2.1).

Some of the events evaluated here have previously been studied to assess impacts to mangroves elsewhere in Australia (Ningaloo Niña 02-03 and Ningaloo Niña 15-16 (El Niños) (See Duke et al., 2017; Lovelock et al., 2017; Asbridge et al., 2019), and in Exmouth Gulf (Cyclone Vance 1999) (see Paling et al., 2008). Climatic events here differ in their associated influence on climate and weather conditions and thus impact on mangroves. Ningaloo Niñas observed are associated with drought and Ningaloo Niños with MHWs and the major potential disturbance for cyclones are wind speed, storm surge and rainfall (Table 2.1).

The comparable events observed also differed slightly. The tropical cyclones included in this study are the most recent cyclones that passed directly through the Exmouth Gulf (Figure 1.1), these cyclones differ in their severity category, with each generating different winds and rain and developing at different times in the year (Table 2.1), in particular, Cyclone Quang developed late in the cyclone season (May). The two more severe cyclones developed during La Niña phases (here Ningaloo Niño 10-11), Cyclone Vance and Carlos, and Cyclone Quang at the beginning of an El Niño phase (here Ningaloo Niña 15-16). In the month at which the cyclones passed Exmouth Gulf, Cyclone Vance had a reported 3-meter storm surge, the other cyclones do not have reported storm surges however this does not mean that they did not occur (Table 2.2). Cyclone Vance and Carlos during this month had higher rainfall and winds recorded than Quang (Table 2.2).

The Ningaloo Niñas studied both occurred during El Niño phases with atmospheric temperature and sea level variables being the most different between these two events

(Table 2.3). During the peak months of the events, average sea level recorded for Ningaloo Niña 15-16 was 20cm lower than Ningaloo Niña 02-03, plus although average atmospheric temperatures recorded at this time were high, Ningaloo Niña 02-03 was associated with anomalously high temperature by almost 3 °C on average (Table 2.3) (Figure 2.2). Ningaloo Niña 15-16 was associated with more rainfall before and after the peak disturbance, than Ningaloo Niña 02-03 (partly due to the co-occurring cyclone), in addition to some rain during the peak event, where during Ningaloo Niña 02-03 the area received very little to no rain (Table 2.3) (Figure 2.2).

The Ningaloo Niños included in this study both generated a MHW during austral summer and occurred close in time, the first occurred in January 2011 caused by a La Niña phase and the second in February 2013 caused by the Australian Summer Monsoon (Table 2.1). This second MHW had a reported 72 consecutive MHW days in this region (December 2012 – Mar 2013) as per Hobday et al., (2016) definition of number of days SSTs are above the 90$^{th}$ percentile of a local threshold. A reported MHW days of the first MHW meeting the same definition cannot be found. SST for the second marine heatwave was on average one degree Celsius warmer during the MHW month, with this event almost 3 °C above normal and the first MHW 2 °C above normal.

**Table 2.1:** Summary of climatic events and dates included in this study and potential disturbance factors associated with each event in addition to climate phases and events they occurred with.

| Event Name | Date(s) | Co-occurred with | Potential disturbance factors |
|---|---|---|---|
| Cyclone Vance | 22 Mar 1999 | La Niña | Severe cyclone<br>• Severe winds<br>• Storm surge (sediment deposition)<br>• High rainfall (flooding) |
| Ningaloo Niña 02-03 | Dec 2002 - Jan 2003 | El Niño | Drought<br>• High (plus anomalously high) air temperatures<br>• Anomalously low SST<br>• Anomalously low sea level<br>• No rainfall |
| Ningaloo Niño 10-11 | May 2010 - Mar 2011 | La Niña (MHW) & Cyclone Carlos | MHW - Thermal stress<br>• Anomalously high SST<br>• High air temperature<br>• Anomalously high sea level<br>• High rainfall (flooding) |
| Cyclone Carlos | 22 Feb 2011 | Ningaloo Niño 10-11 | Severe Cyclone<br>• Severe winds<br>• High rainfall (flooding)<br>• No reported storm surge |
| Ningaloo Niño 12-13 | Dec 2012 - Mar 2013 | Australian summer monsoon (MHW) | MHW - Thermal stress<br>• Anomalously high SST<br>• High (& anomalously high) air temperatures |
| Cyclone Quang | 1 May 2015 | Ningaloo Niña 15-16 | Cyclone<br>• High wind speeds<br>• High rainfall (flooding)<br>• No reported storm surge |
| Ningaloo Niña 15-16 | Apr 2015 - Apr 2016 | El Niño & Cyclone Quang | Drought<br>• Anomalously low sea level<br>• High air temperature<br>• Anomalously low SST<br>• Little rainfall |

**Table 2.2:** Tropical cyclone event summaries at the time or for the month (total rainfall) that they passed over Exmouth Gulf. See dates in Table 2.1.

| | Category | Max wind 10min(km/h) | Max wind gust (km/h) | Storm Surge (m) | month Rainfall total (mm) |
|---|---|---|---|---|---|
| Cyclone Vance 1999 | 5 | 175.9 | 267.0 | 3.6 | 217.0 |
| Cyclone Carlos 2011 | 2 | 92.6 | 129.6 | NA | 218.2 |
| Cyclone Quang 2015 | 1 – TL* | 37.0 | 83.3 | NA | 117.0 |

*Tropical Low

**Table 2.3:** Ningaloo Niño/Niña impact event summaries for the month considered the peak disturbance, where mean sea surface temperature (SST), mean maximum air temperature (Max Air Temp), and sea level are climate averages for the month and rainfall which is the total rainfall for the peak disturbance month. Peak disturbance months for each event are identified in Figure 2.2 and 2.3, where January is considered the peak disturbance month for all events except Ningaloo Niño 12-13 which is considered in February.

| Event | Impact | SST (°C) | Max Air Temp (°C) | Sea Level (m) | Rainfall (mm) |
|---|---|---|---|---|---|
| Ningaloo Niña 02-03 | Drought | 27.1 | 40.9 | 1.4 | 0 |
| Ningaloo Niño 10-11 | MHW* | 30.3 | 36.6 | 1.8 | 100.8 |
| Ningaloo Niño 12-13 | MHW* | 31.5 | 40.0 | 1.7 | 1.0 |
| Ningaloo Niña 15-16 | Drought | 27.0 | 35.1 | 1.2 | 0.6 |

*marine heat wave

## 2.3 Data and pre-processing

### 2.3.1 Climate data

Climate data were examined to identify peak disturbance dates, indicated by high or low climate anomalies, to guide acquisition of remote sensing data (see section 2.3.2). The climate data can also help to understand potential climatic drivers of decreases or increases in mangrove fraction (or proportion of loss) associated with each climatic event. Climate data were acquired from 1998, or as early as available, to 2020. Climate anomalies were calculated by subtracting monthly measurements from the long-term average for that month. Almost all climate data were retrieved from the Bureau of Meteorology (BOM), with monthly rainfall and air temperature acquired from Learmonth Airport station (Station 005007), and monthly sea level data from BOM's sea level gauge within Exmouth marina. Daily SST data was extracted from remotely sensed data from the Physical Oceanography Distributed Active Archive Centre (PO.DAAC) repository from the National Aeronautics and Space

Administration (NASA) (NASA, 2021). The Multi-scale Ultra-high resolution (MUR) SST dataset used combines several sensors including MODIS, AMSR-E and AVHRR-3 at varying spatial scales merged for 0.01 degree spatial and daily temporal resolution (NASA, ND). SST was extracted at approximately five equally spaced points along the eastern Exmouth Gulf and averaged.

### 2.3.2 Remote sensing data and selection criteria

Mangrove response to climatic events was evaluated at the landscape scale using atmospherically corrected satellite remote sensing images from Landsat 5 (TM), Landsat 7 (ETM) and Landsat 8 (OLI) (USGS, 2021; USGS 2021). This Landsat data provides spatial resolution of 30 meters and a 16-day return rate with an overpass time of around 10:15am. These Landsat satellites also collectively provide over 30 years of consistent measurements which is essential for this study type. Data imagery were obtained from USGS Earth Explorer Collection 2 Level-2 Science Products (https://earthexplorer.usgs.gov/) (path 115 and rows 75 and 76) between 1998 to 2021 and processed using ENVI software.

To reduce impacts of seasonality on mangroves when detecting impacts and tracking recovery, images were acquired from the same time of year. To detect impact, images (from the same Landsat sensor for a given climatic event) were selected before and after the time of the peak impact (see Figure 2.2 & Figure 2.3), and day of passing for tropical cyclones. For the Ningaloo Niño/Niñas, image dates were in July/August (with one exception acquired 1st September). For cyclones, images were acquired within two months before and after the cyclone. All image dates for tropical cyclones were within the first half of year when the only rainfall during this time is directly attributed to the event itself, therefore no large variation should be attributed to difference in seasonality.

To evaluate recovery, annual images (from any Landsat) were acquired from July/August. This image timing corresponds to the peak growing season following the month with the most reliable high rainfall (BOM, 2021), which is when mangroves are most phenologically consistent (Coupland et al., 2005; Pastor-Guzman et al., 2018). Cloud free data images were prioritised within the two-month time frames.

A portion of the Landsat 7 (ETM) data used in this study had stripes of no data due to a scan line corrector error that occurred in 2003 (Markham et al., 2004). To combat the effects of no

data stripes on the study, when it was necessary to use Landsat 7 data, two images from the two-month time that collectively provided full data coverage (hence force, dual images) were acquired to represent each year. However, when Landsat 5 or Landsat 8 data were available, these images were prioritised over Landsat 7. Landsat acquisition dates can be seen in Appendix A. The final dataset was an image series with annual images from July/August for the time frame 1998-2021, including extra image dates for the years with cyclones.

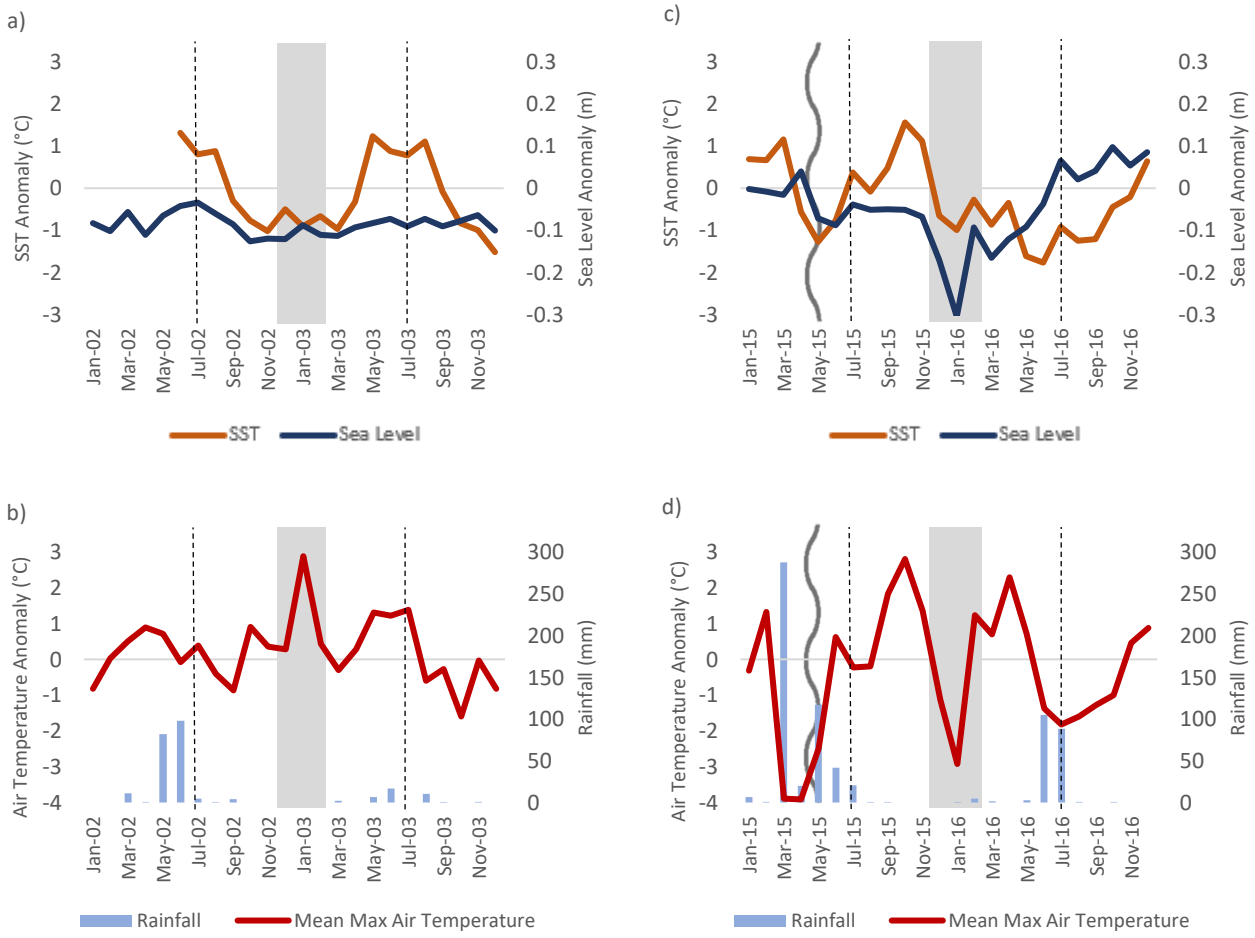


**Figure 2.2:** Climate Anomaly data for drought events, including sea surface temperature (SST) and sea level (a), mean maximum air temperature and total monthly rainfall (b) for Ningaloo Niña 02-03 and sea surface temperature (SST) and sea level (c), mean maximum air temperature and total monthly rainfall (d) for Ningaloo Niña 15-16, where grey panels indicate the potential peak disturbance, the dark grey wavy line a cyclone and the Landsat image acquisition indicated by black dotted lines.

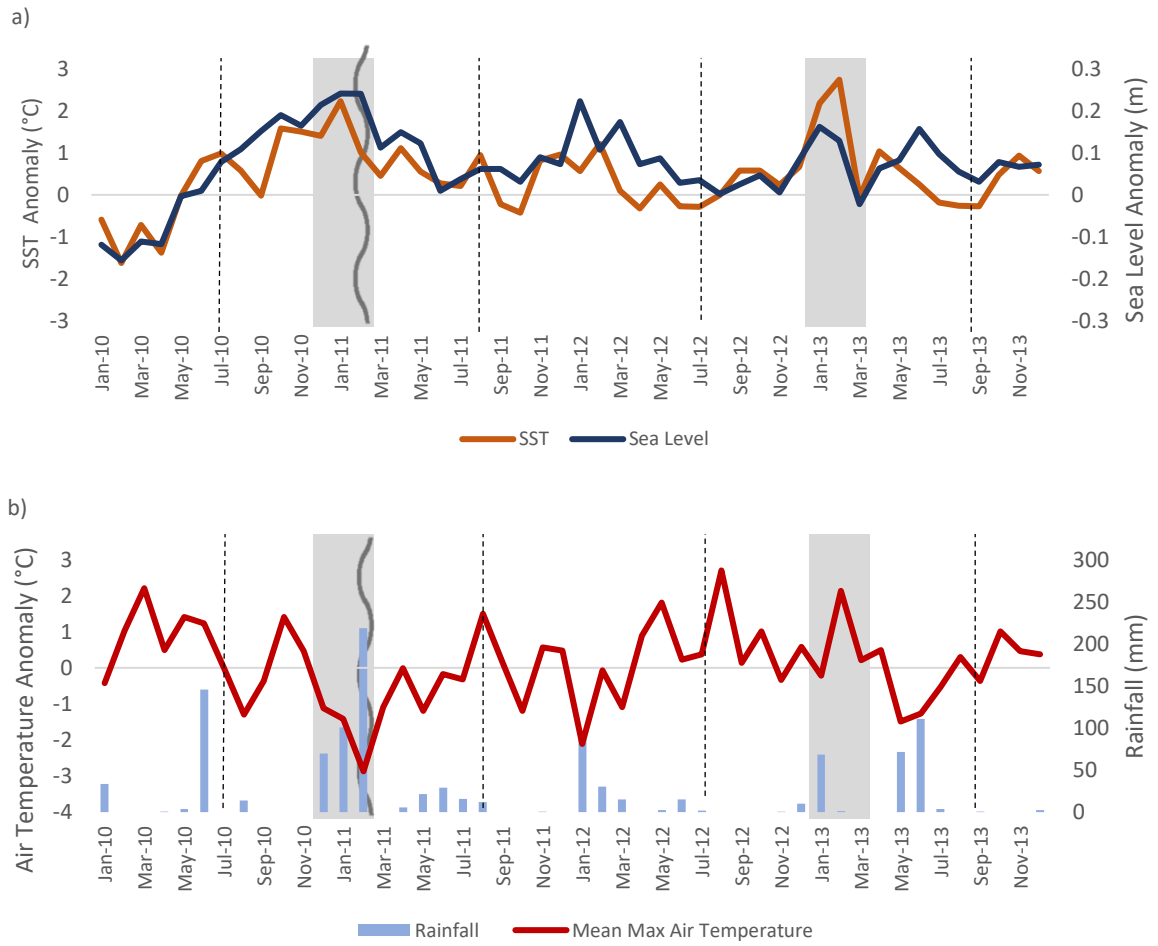


**Figure 2.3:** Climate anomaly data for MHW events, including sea surface temperature (SST) and sea level (a), mean maximum air temperature and total monthly rainfall (b) for Ningaloo Niño 10-11 and Ningaloo Niño 12-13, where grey panels indicate the potential peak disturbance, the dark grey wavy line a cyclone and the Landsat image acquisition indicated by black dotted lines.

## 2.4 Multiple Endmember Spectral Mixing Analysis (MESMA)

A mixed pixel is a result of multiple land cover types present within one pixel. Common methods to quantify vegetation cover, such as vegetation indices, are unable to discriminate vegetation types within a given pixel or across an image and thus unable to distinguish mangrove cover from vegetation cover overall. Spectral unmixing overcomes these shortfalls through its ability to deal with mixed pixels and determine proportions of land cover types per pixel rather than a general greenness index (Thayn, 2020). Spectral Mixture Analysis (SMA) models the pixels of an image as a linear combination of spectra from pure pixels of each class (endmembers), estimating the relative proportion within each mixed pixel that is made up of that class (Adams et al., 1993). This analysis results in a fraction image per land cover type, showing the proportional cover by each land cover class within each pixel. This is

traditionally done using a fixed set of endmembers, with one per broad land cover class, thus failing to account for variability within a land cover class (Roberts et al., 1998). Multiple Endmember Spectral Mixture Analysis (MESMA), an extension of SMA, addresses this limitation of SMA by allowing for multiple endmembers per land cover class capturing variability across a landscape and within classes (Roberts et al., 1998). MESMA also enables the number and type of endmembers used to model a pixel's reflectance to vary, as it tests all combinations of endmembers on each pixel, which minimises model error based on lowest Root Mean Squared Error (RMSE) (Roberts et al., 1998). MESMA has not been applied in many marine coastal settings. One study suggests MESMA is more effective in these environments than SMA due to its ability to account for variation of classes due to tidal levels (He et al., 2010).

The MESMA procedure consists of three steps: building a spectral library of candidate endmembers for the land cover types present in the study area, selection of the optimal endmembers, and then running MESMA to decompose the mixed pixels and calculate fraction images. The following sections of the methods follow the scheme indicated in Figure 2.4.

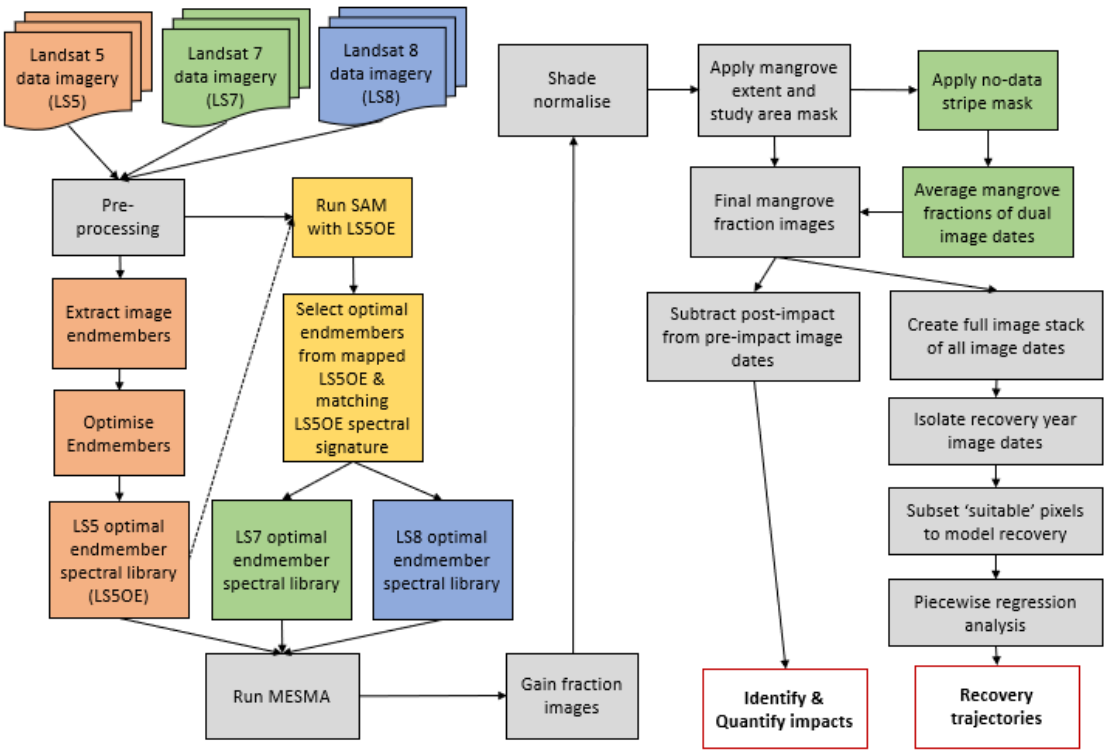


**Figure 2.4:** Flowchart of methods covering the sections of methods that follow, where procedure applied to Landsat 5 is indicated by orange, to Landsat 7 by green, Landsat 8 by blue, to Landsat 7 and 8 by yellow and to all by grey. Outcomes are indicated by white boxes.

### 2.4.1 Endmember selection

Endmember selection is arguably the most important part in the MESMA procedure. Endmembers may be collected from the field, laboratory, or directly from images. Image endmembers were used for this research. Using image endmembers has two advantages, they are easily obtained and once obtained they will have the same scale of measure as the data being modelled.

This study utilised multiple resources to identify land cover classes within the study area and help build the spectral library needed to conduct a MESMA. Firstly, a thorough environmental report on the mangrove and coastal ecosystem of the eastern Exmouth Gulf from 2005 was used as reference material for the study area (Humphreys et al., 2005). Land cover maps in the report from 4$^{th}$ August 2005 were cross-referenced with a Landsat image from the assembled data series that was the closest in time to the surveys in the report (01-07-2005). Another environmental report completed for this area as part of the same project but with a focus on vegetation was used for better description of saltmarsh areas (McCreery et al., 2005). Google images (Maxar Technologies, Map data 2021) and satellite images from within ArcGIS (appeared to be higher resolution), were also used to help identify landcover types from the remote aspect. Photographs from around the study area taken in 2004 (Photo credit E. Paling) were observed to get a closer understanding of the study area. Lastly, the 2D scatter plot function within ENVI was also utilised (between red and NIR bands) to spectrally separate land cover types and identify purest pixels of each class. These are pixels that fall at the outside corners of the point cloud in a scatter plot. A reference 2D scatter plot from within the study area was also available for comparison to confirm that groupings of classes in the spectral scatter plot was correct (Humphreys et al., 2005 - Appendix 2). Upon review of these resources and familiarisation with the image date five land cover classes were selected for the analyses, including mangroves, algal mat, saltmarsh, water and bare (e.g. sand, mudflats).

Endmember selection was concentrated across three distinctive regions of the study area, in the north, central and southern regions, ensuring representatives from across the landscape and accounting for any variability from north to south on the 01-07-2005 image date. Another image date (pre-disturbed) in the series was also used to ensure the full range of variability was represented by candidate set of endmembers. The candidate endmember selection was focused on representativeness of a land cover type (i.e. mud, mangrove, sand algal mat etc.)

from each distinctive region of the study area. Various endmembers from within each landcover class were collected, this included sparse, dense, partially inundated (due to tide or rainfall), and dry vegetation for mangrove, saltmarsh and algal mat classes, endmembers from seaward and landward margins (including around creeks) for these classes, as well as dry and partially inundated mudflats, sand and supratidal land for bare endmembers, and variable turbidity and depth for water endmembers. In addition, dead mangrove endmembers and dry algal mats (not active), were collected as bare endmembers. If the spectra from a pixel was considered too unusual it was not included. In total the spectral library contained 169 candidate endmembers, including 31 mangrove, 26 algal mat, 14 saltmarsh, 33 water and 65 bare.

### 2.4.2 Optimisation of endmembers

The second critical step is optimisation of endmembers to increase the effectiveness and computational efficiency of MESMA. Common metrics of endmember quality were used to select optimal endmembers from the full library, the Endmember Average RMSE (Root Mean Squared Error) (EAR), Minimum Average Spectral Angle (MASA) and the Count Based endmember selection (CoB) metrics In_CoB and Out_CoB (see Table 2.4). A combination of these is best as some of these metrics are sensitive to certain factors compared to the others for example dark and light objects. Optimisation was run on the entire merged spectral library. Endmembers with high Out_Cob values were considered erroneous and discarded (Table 2.4). Following this, endmembers were optimised for Landsat 5 data and used to find matching endmembers for Landsat 7 and 8 data, as described below.

**Table 2.4:** Metrics of endmember quality used to find optimal endmembers where EAR (Endmember Average RMSE), MASA (Minimum Average Spectral Angle), CoB (Count Based endmember selection).

| Metric | Description |
|---|---|
| EAR | EAR identifies the endmember that produces the lowest average RMSE when it is used to model all the other spectra within that same class in the endmember library.[1] |
| MASA | Spectral angle is the angle between the spectra. MASA measures the minimum average spectral angle between spectra to determine the endmember that best models each class by identifying which endmember has the lowest average spectral angle within the same class.[2] |
| CoB | CoB selects endmembers based on which modelled the greatest number of spectra within their own class (In_CoB).[3] Thus most representative of their class. CoB also identifies endmembers that model spectra outside of its class (Out_CoB) (erroneous).[3] |

[1](Dennison & Roberts, 2003), [2](Dennison et al., 2004), [3](Roberts et al., 2003).

#### *3.4.2.1 Optimisation of endmembers for Landsat 5*

The spectral library was run through optimisation several times to remove all erroneous spectra (high Out_CoB values). Then the endmembers with the highest In_CoB values and the lowest EAR and MASA values were selected for each class as potential optimal endmembers. The spectral signatures of this refined set of endmembers were manually screened to identify any spectra that were too similar, in which case the one with the lowest EAR, MASA and highest In_CoB value was retained. This resulted in 5 mangrove, 7 algal mat, 4 saltmarsh, 10 water and 12 bare optimal endmembers.

For consistency across the study the optimal endmembers from Landsat 5 were used to guide endmember selection for Landsat 7 and 8. Landsat 8 has an extra spectral reflectance band (B1 Aerosols) and although Landsat 5 and 7 have the same number of spectral reflectance bands there are slight differences in wavelength ranges (0.01µm) for a couple of the bands. Therefore, for robustness this study developed separate spectral libraries to analyse data from each Landsat satellite.

#### *2.4.2.2 Optimal endmember selection for Landsat 7 & 8*

Due to the overlap in operation times between Landsat 5 and 7, a Landsat 7 image date from the same time as the image date used for endmember collection for Landsat 5 can be used. The closest Landsat 7 image date with no issues was 25 days later. Initially, spectra were extracted from the same locations as the set of optimal endmembers identified in the contemporary Landsat 5 images for Landsat 7. However, after 25 days, due to some rainfall (55.2mm in total) and sea level variability there were considerable changes in reflectance signatures at some of these pixels. Thus, it was unclear that the same locations would optimally span endmember space for Landsat 7. In cases where there were changes at a given pixel from the optimal set of Landsat 5 endmembers, new spectra from the Landsat 7 image that were most spectrally similar to the Landsat 5 endmember were identified using Spectra Angle Mapper (SAM). This method was followed exclusively to develop optimal endmembers for Landsat 8.

SAM is a spectral classification that matches pixels to reference spectra, by calculating the spectral angle between spectra to determine spectral similarity (Kruse et al., 1993). SAM was used to find consistent spectra to the optimal set for Landsat 7 and Landsat 8. Pixels that were

selected as consistent spectra and that were the most similar in spectral shape (i.e. spectral angles) and reflectance compared to the optimal set were selected as optimal endmembers for Landsat 7 and 8. For Landsat 8, this method was used on the earliest image date visually most similar (i.e. due to an active algal mat) to the Landsat 5 2005 image date and for the same time of the year (i.e. July). Correlations were run on mangrove fraction images between the Landsat 5 image date and the image dates used for consistent spectra for Landsat 7 and 8, with correlations of 0.78 and 0.77 respectively, showing high correlations between image dates used for consistent spectra to the Landsat 5 image date.

Preliminary MESMA analyses were run on all image dates (see section 2.4.3) and screened to assess endmember performance. 2- 3 and -4 endmember models were also tested, however the extra complexity was not needed. A shade endmember is always assumed within all the models (e.g. 2 EM model = shade + mangrove, 3 EM model = shade + mangrove + water). Spectral signatures of pixels within patches classified as non-mangroves adjacent to mangroves were assessed to ensure the endmembers had not missed mangroves. When mangrove patches were missed their spectral signatures were assessed and compared to the existing optimal mangrove endmember library to determine why they had not been detected by the MESMA. Mangroves patches not accounted for in the initial set of optimal endmembers were healthy mangroves (high NIR) that included some fringing areas, and that were partially inundated due to high sea level in those image dates. New endmembers were collected to capture this variability (n=6) and added to the existing set of optimal endmembers for each Landsat. The final optimal endmembers resulted in 11 mangrove, 7 algal mat, 4 saltmarsh, 10 water and 12 bare. See final optimal endmembers in Figure 2.5.

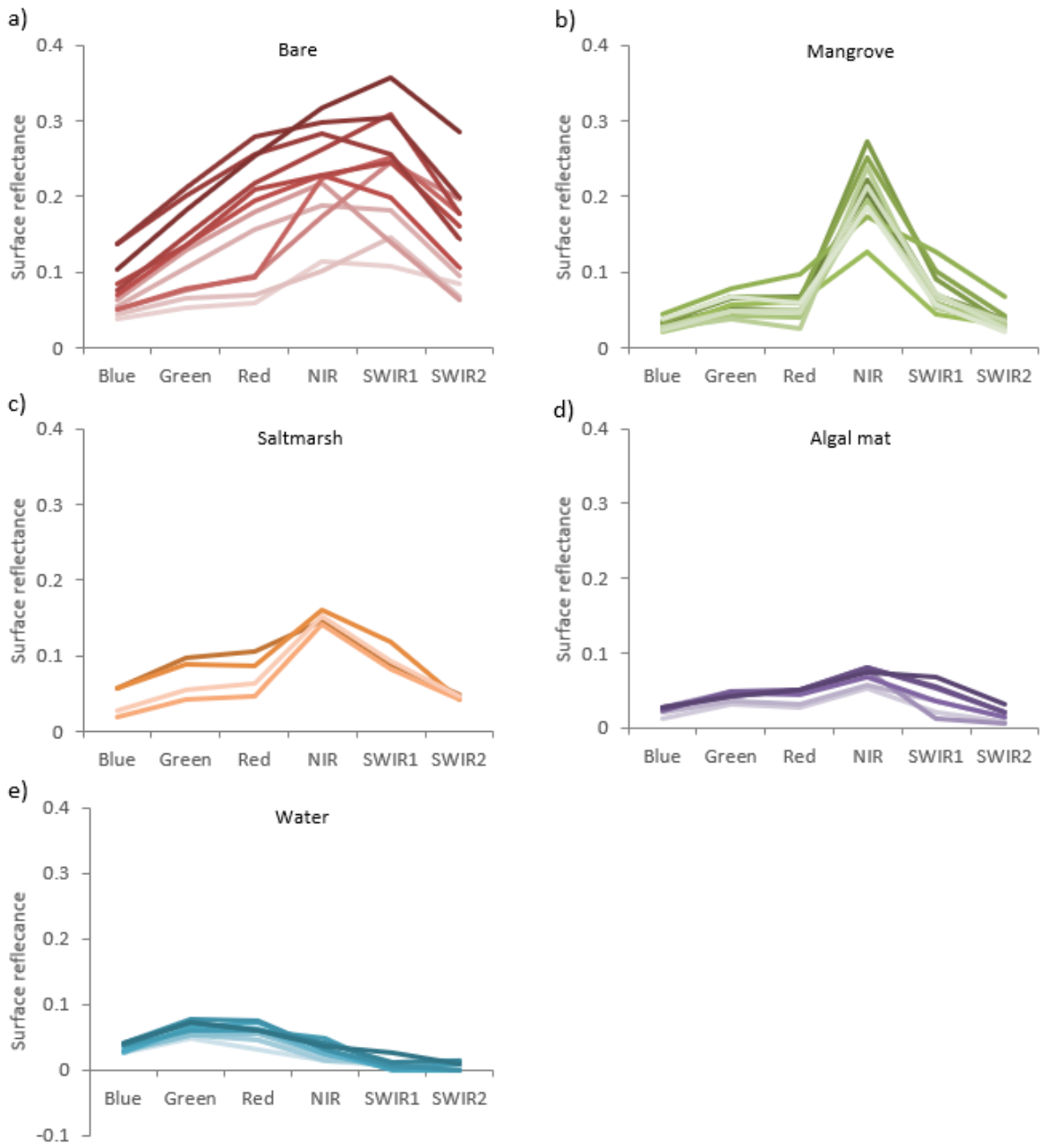


**Figure 2.5:** Final optimal endmember spectra for bare (a), mangrove (b), saltmarsh (c), algal mat (d) and water (e) land cover classes used for MESMA (n = 44). Where bare endmembers consist of different statuses of mudflat and beach sand, supratidal ground, dead mangroves, and dead/dry algal mats. Mangrove endmembers include sparse and dense groupings and variable contributions of water due to tide. Saltmarsh endmembers tended to include dry sparse representatives, whereas algal mat endmembers were active and dense and varied in status due to rain or position on the tidal margin. Water endmembers consisted of different depth and turbidity.

### 2.4.3 Application of MESMA

MESMA analyses were run with 2 and 3 endmember models, which are typically the best levels of complexity for natural and disturbed systems (Powell & Roberts, 2008; Wang et al., 2014). This resulted in 797 models run on each pixel to determine the best model to spectrally

unmix the pixel based on constraints set. The default constraints were accepted, which are informed by the literature (see Table 2.5), these constraints set the tolerances around the allowed fraction values so that they make sense, ensure small error and influence decisions around the complexity of the model selected (e.g. 2 or 3 EM model). Each Landsat dataset was run through MESMA separately. MESMA processing was completed using Viper Tools software (V3.0) (https://sites.google.com/site/ucsbviperlab/), an open-source extension to ENVI image processing software.

Mangrove fraction images developed from MESMA were post-processed in R (V3.6.1) to apply shade normalisation and to mask pixels outside the study area and mangrove extent. An inclusive mangrove extent mask was developed for each image date, created using NDVI (normalised difference vegetation index) and the sum of all Landsat bands (less B1-Aerosols for Landsat 8). An NDVI of above 0.12 and summed brightness between 5000 and 7200 was used as an inclusive threshold for mangroves to remove pixels that were non-vegetation and areas that were too dark (e.g. water) and too bright (e.g. sand) and ideally mainly mangrove. In addition to a mangrove extent mask calculated for each image date post-processing included aggregating the two Landsat 7 image dates by selecting the pixel value with data, in the case of no-data stripes, and averaged the two pixel values for data coverage in both dates resulting in one mangrove fraction image for the dual dates.

**Table 2.5:** MESMA default constraints used in Analysis.

| Constraint | Metric | Details |
|---|---|---|
| Minimum Fraction | -0.05 | Allows fraction images to identify fractions as low as this figure (5% lower). |
| Maximum Fraction | 1.05 | Allows fraction images to identify fractions as high as this figure (5% higher). |
| Minimum shade fraction | 0.00 | The minimum fraction of photometric shade applied to a pixel for the shade endmember. |
| Maximum shade fraction | 0.80 | The maximum fraction of photometric shade applied to a pixel for the shade endmember. |
| Maximum RMSE | 0.025 | The maximum RMSE (root mean squared error) allowed for a modelled pixel, if higher pixel left unclassified. |
| Fusion Threshold | 0.007 | Indicates the improvement needed in RMSE to select a more complex model, otherwise a less complex model is used. |

## 2.5 Change analysis

### 2.5.1 Impact detection and quantification

Change detection was run on mangrove fraction images by subtracting the mangrove fraction images from before and after the potential disturbance and thresholding impacts to account for natural variation and identify high impacts (Table 2.6). The standard deviation of mangrove fraction change between consecutive years with no climate disturbance was used as the threshold to distinguish between natural variation, and between large and small changes in mangrove fraction (Table 2.6). For comparison between climatic events, the extent of the impact was calculated as the proportion of mangrove pixels (determined from the pre-impact mangrove extent mask) and thus area within each change class. This was also calculated for the north, central, and south regions of the study area, and for different distances from the coast in 200m margins one kilometre landward. Mangrove fraction change detection was analysed in ENVI.

**Table 2.6:** Categorisation of mangrove fraction change from pre- and post-image dates for impact detection analysis.

| Fraction change | Change Class |
|---|---|
| < -0.667 | High decrease |
| -0.334 – -0.667 | Low decrease |
| -0.333 – 0.333 | Natural variation |
| 0.334 – 0.667 | Low increase |
| > 0.667 | High increase |

### 2.5.2 Recovery

Climatic events that occurred early enough to have 10 years of recovery data were observed for recovery, including only those that had an apparent negative impact. This included Cyclone Vance, Ningaloo Niña 02-03 and Ningaloo Niño 10-11 which encompasses Cyclone Carlos. To evaluate mangrove recovery from studied climatic impacts, all image dates were stacked into a single image and recovery was tracked using July/August image dates only. A piecewise regression analysis was used to estimate the temporal trajectory of mangrove fraction recovery over a ten-year time frame for all suitable pixels, where the first year is the July/August image date before the impact. Suitable pixel to track recovery were identified by calculating adjusted R square (to assess model fit), adjusted to account for short recovery time frame, amount of data (i.e. number of years with a mangrove fraction) and whether there was a decline in mangrove fraction and thus a negative impact (to track a recovery), see thresholds in Table 2.7.

Recovery analyses conducted as part of this investigation included identifying overall increasing and decreasing trends in recovery, measured by initial trajectory (hereafter initial recovery) (slope 1), and the following trajectory (slope 2), with the calculated slope of these trajectories, indicating a recovery rate per year (Figure 2.6). The 'breakpoint' in these temporal trajectories, which included at what year and at what mangrove fraction, were also calculated (elbow in trend) (Figure 2.6). The time frame of recovery was also calculated as the year the overall trajectory trend (i.e. slope 1 or 2) was greater than the pre-disturbed mangrove fraction (Figure 2.6). As part of the results only slope 1, the initial trajectory of mangrove recovery, and recovery time (years to recover) are reported here, where certain aspects of mangrove recovery may not be accounted for as indicated in Figure 2.6. The piecewise regression analyses were conducted in R (V4.0.3) (package 'segmented') (CRAN, 2021).

**Table 2.7:** Metrics to be met to be considered a suitable pixel for recovery analysis.

| Metric | Threshold | Description |
|---|---|---|
| Negative impact | Post-mangrove fraction < pre-mangrove fraction, and impact < -0.333 (decrease > 0.333) | To ensure only pixels negatively impacted, and outside of natural variation, are assessed for recovery. |
| Adjusted R Square | > 0.40 | To ensure mangrove recovery trajectories are adequately modelled (piecewise slopes are well fitted to mangrove fraction trajectories). |
| Enough data | 5/10 years contains mangrove fraction | Must be at least 5 years of mangrove fraction data, to properly model mangrove trajectories and to limit modelling algal mat or salt marsh |

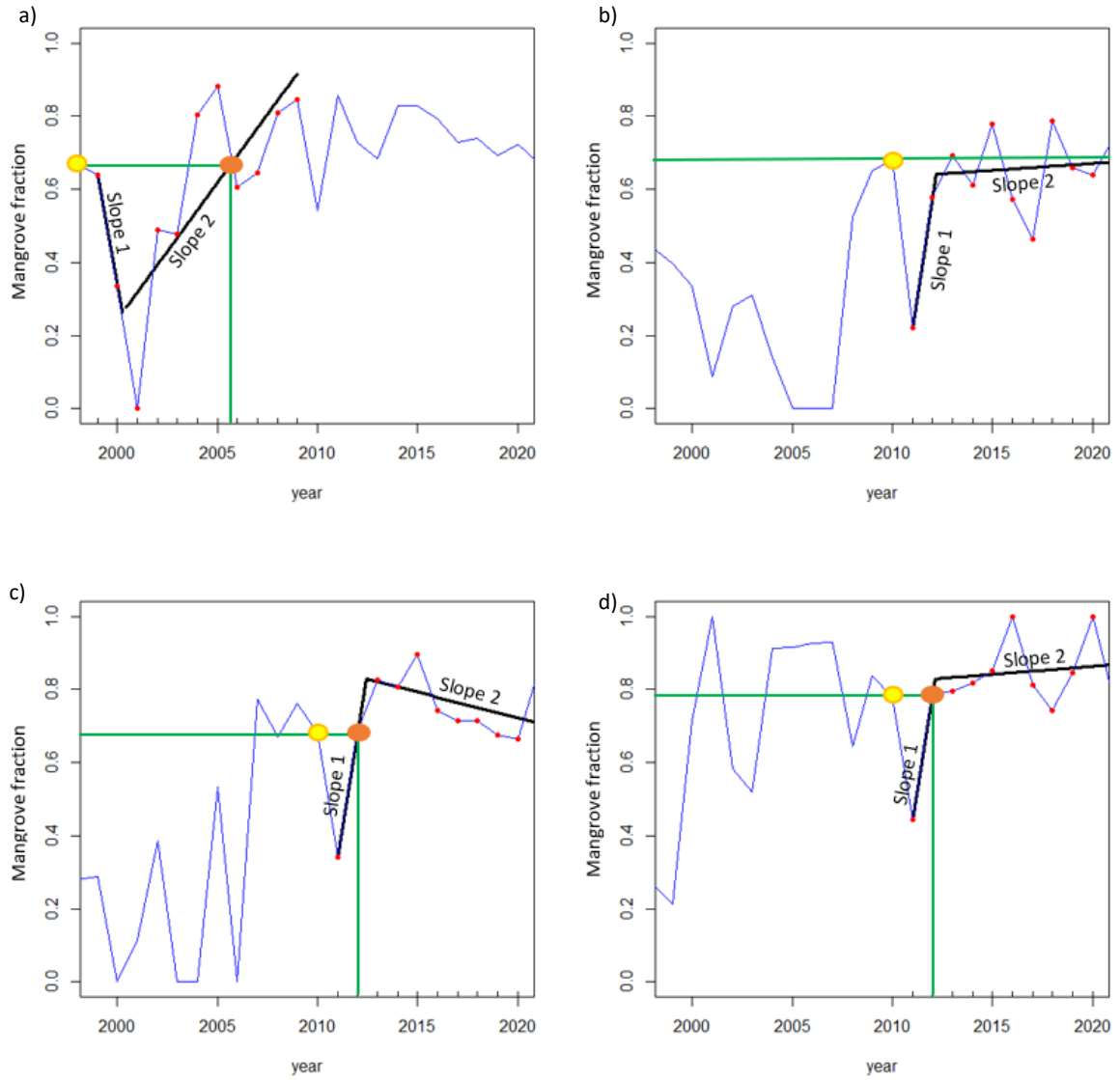


**Figure 2.6:** Sample mangrove fraction pixel trajectories using piecewise regression which fits the overall mangrove fraction trajectory (recovery) for ten years with one breakpoint (elbow in trajectory, black lines), calculating two slopes in these trajectories, slope 1 and 2 indicated on the plots. Recovery time is indicated by the orange dot and the green vertical line, when the mangrove fraction on the slope (overall mangrove trajectory) is greater than the pre-disturbed mangrove fraction (yellow dot and green horizontal line). Sample trajectories demonstrate several instances where the initial trajectory is in decline then subsequent increase with recovery identified on slope 2 (a), two increasing trends in recovery however not yet recovered (b), initial increase with recovery identified however followed by subsequent decrease (c), and initial recovery with recovery identified then subsequent further moderate increase (d). All sample recovery models have met suitability pixel constraints.

# 3.0 Results

## 3.1 Impacts

### 3.2.1 Whole study area impacts

Mangrove response to extreme climatic events investigated varied in quantity, area and magnitude of impact. Overall, most of the negative impacts were associated with tropical cyclones and drought events (Figure 3.1 and Figure 3.2). MHWs were not associated with as much negative impact (Table 3.1 and Figure 3.3). Negative impacts resulting from cyclone and drought events also resulted in more high magnitude decrease (mangrove fraction decrease by over 0.667) in mangrove fraction.

Cyclone Vance 1999, a category 5 cyclone associated with the highest wind speeds, storm surge and rainfall had the largest negative impact on mangroves compared to all other events captured by this study (Figure 3.1, Table 3.1, and Figure 3.3). Cyclone Vance caused a decrease in mangrove fraction over 51.64% (79.42 $km^2$) of the study area, and the largest proportion of area with high decrease in mangrove fraction (19.06%) within 2 months (Table 3.1 and Figure 3.1). The second largest impact was following the first drought event, Ningaloo Niña 02-03, resulting in a proportional area of 34.66% (38.91$km^2$) decrease in mangrove fraction. Cyclone Quang and a drought event, Ningaloo Niña 15-16, contributed to the other largest impacts (16.60% - 14.50$km^2$ and 13.15%- 16.52$km^2$, respectively) some 12 and 13 years after Ningaloo Niña 02-03 (Table 3.1 and Figure 3.1).

The largest proportion of increases in mangrove fraction were attributed to all three tropical cyclones, with high increase most predominantly associated with Cyclone Quang (Table 3.1 and Figure 3.1). The drought and MHW events, Ningaloo Niño/Niñas, contributed little to stimulating mangrove fraction increases. Ningaloo Niña 15-16 resulted in marginally larger mangrove fraction increase for these events, however this could be partly due to the co-occurring Cyclone Quang. It is however apparent that some of the areas experiencing high mangrove fraction decrease and increase following Cyclone Carlos and Quang were in areas generally dominated by algal mats (areas separate to mangroves communities on the coast in mapped figures), most evident after Quang (Appendix B - Figure B.1 and Figure B.3).

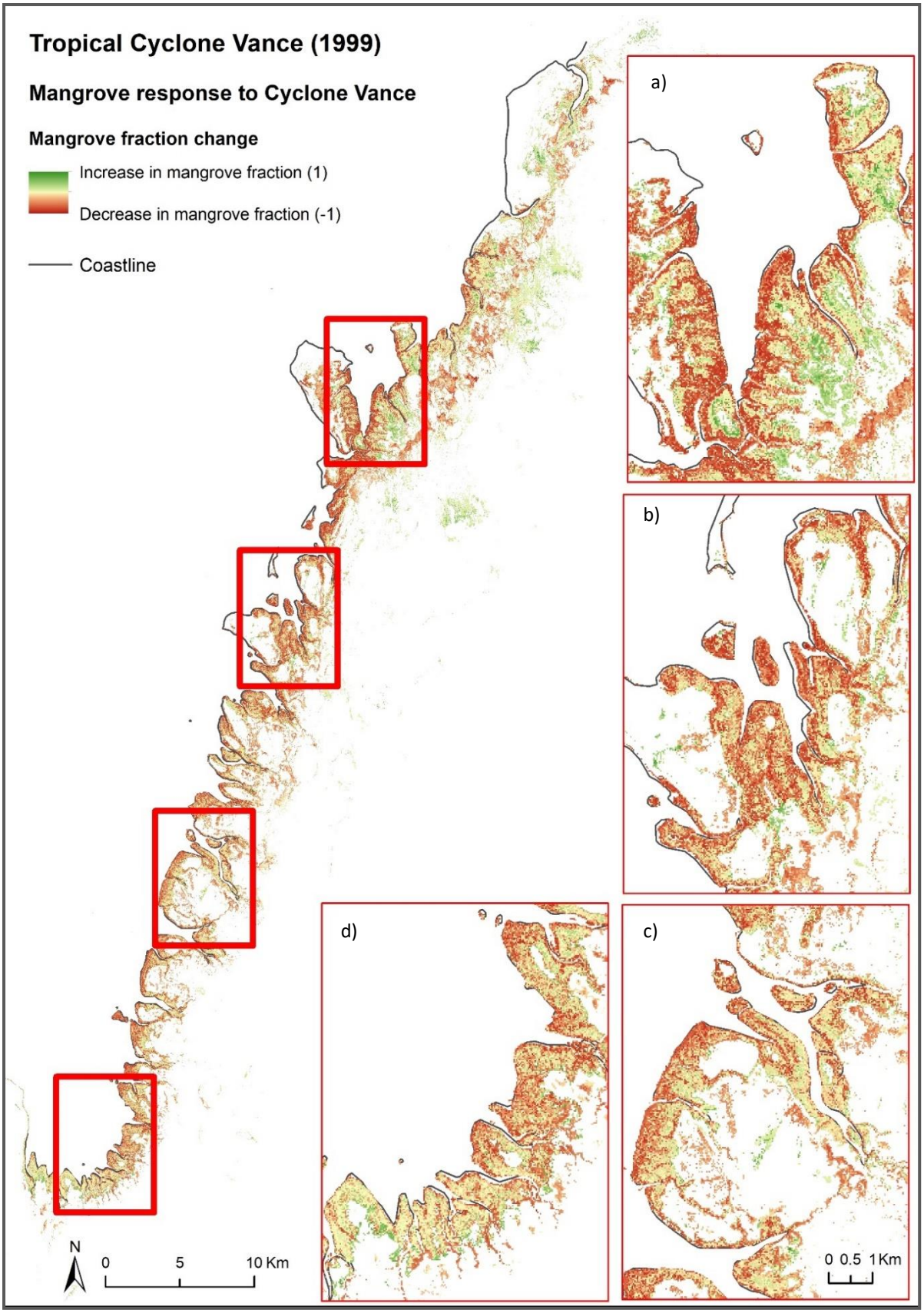


**Figure 3.1:** Mangrove fraction change map following Tropical Cyclone Vance where reds indicated mangrove fraction decreases and greens indicate mangrove fraction increases, including zoom insets of part of the northern (a), upper central (b), lower central (c), and southern localities of the study area. The scale of all insets is the same as in inset (c).

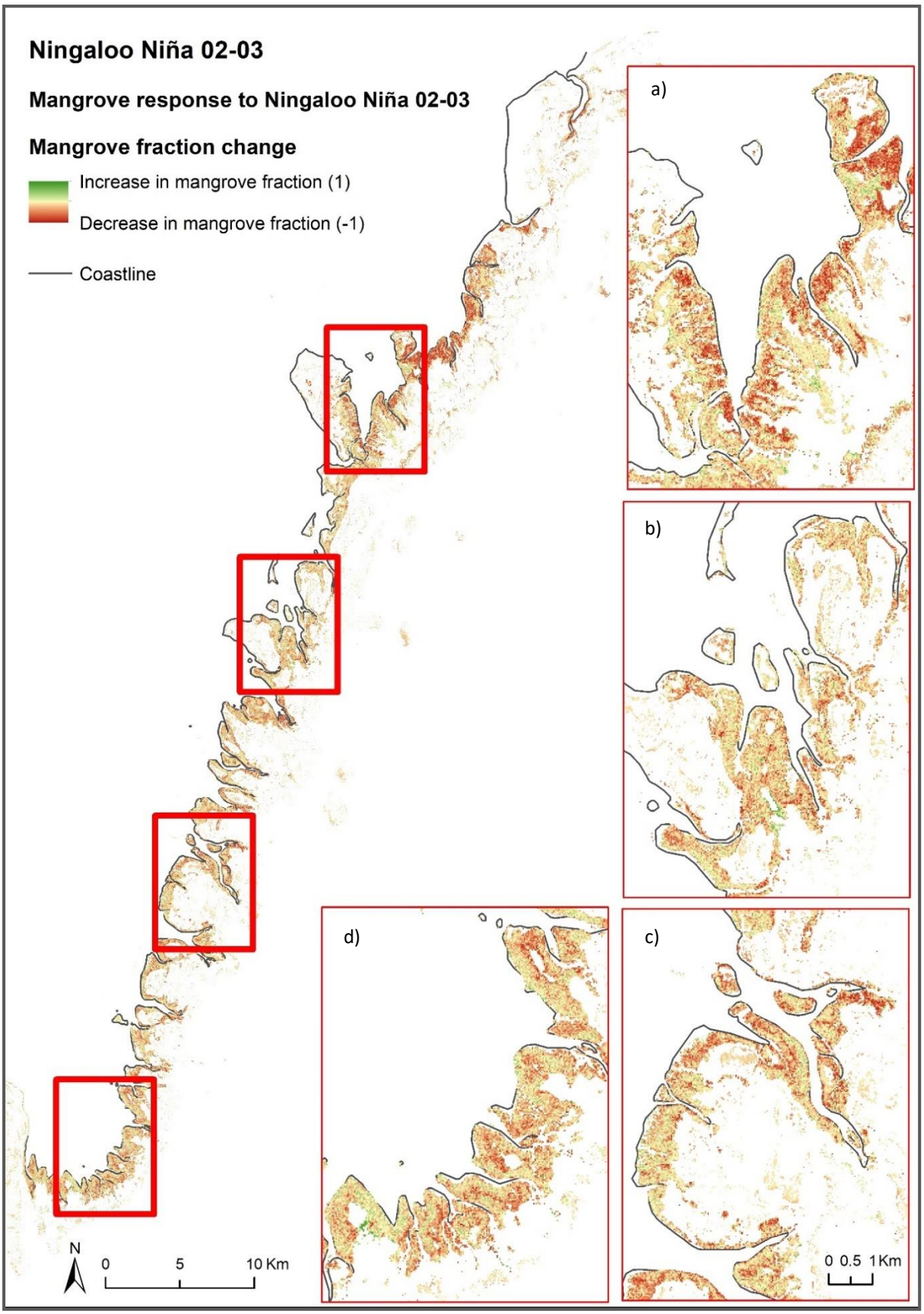


**Figure 3.2**: Mangrove fraction change map following Ningaloo Niña 02-03 where reds indicated mangrove fraction decreases and greens indicate mangrove fraction increases, including zoom insets of part of the northern (a), upper central (b), lower central (c), and southern localities of the study area. The scale of all insets is the same as in inset (c).

**Table 3.1:** Total proportion and area of decreases and increases in mangrove fraction across the entire study area presented in chronological order, with the three highest total proportion of decreases and increases of mangrove fraction shaded grey. Mangrove fraction change are proportional to the pre-impact image date of mangrove fraction for the study area for each respective climatic event.

| | Decreases | | Increases | |
|---|---|---|---|---|
| Climatic event | Proportion (%) | Area ($km^2$) | Proportion (%) | Area ($km^2$) |
| Cyclone Vance | 51.64 | 79.42 | 9.39 | 14.45 |
| Ningaloo Niña 02-03 | 34.66 | 38.91 | 6.29 | 7.06 |
| Ningaloo Niño 10-11 | 11.36 | 30.76 | 5.47 | 37.46 |
| Cyclone Carlos | 11.66 | 13.06 | 19.13 | 8.57 |
| Ningaloo Niño 12-13 | 7.90 | 18.37 | 5.19 | 10.84 |
| Cyclone Quang | 16.60 | 14.50 | 20.22 | 6.98 |
| Ningaloo Niña 15-16 | 13.15 | 16.52 | 7.76 | 27.10 |

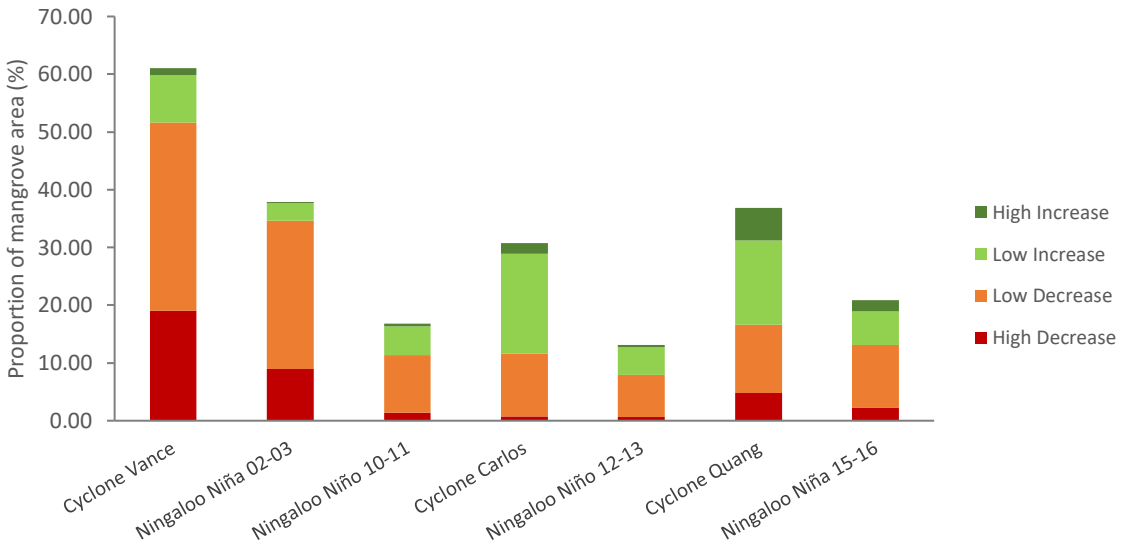


**Figure 3.3:** Proportion of mangrove area experiencing fraction increase and decrease per change class across the entire study area for each climatic event in chronological order. Mangrove fraction change are proportional to the pre-impact image date of mangrove fraction for the study area for each respective climatic event.

### 3.1.2 Impacts across regions of the study area

Spatial patterns observed in Figures (3.1, 3.2 and 3.3) show that some of the climatic impacts have resulted in larger negative or positive impacts across different regions of the study area. Although for some of the individual events investigated there is clear spatial discrimination of negative impact, there does not appear to be a clear regional distinction for alike climatic

disturbances. However, the most severe impacts, Cyclone Vance and Ningaloo Niña 02-03, had the largest proportion of area with a decrease in mangrove fraction in the central and north regions respectively, with the lowest mangrove fraction decrease by 10 percent in both cases occurring in the south region. The north region was only marginally less affected by Vance than the central region. This is particularly evident for Ningaloo Niña 02-03 in the north region, just north of the area captured by inset (a) in Figure 3.2, where that portion of the coastline appears to have the highest magnitude of mangrove fraction decrease. Conversely for the comparable event, Ningaloo Niña 15-16 resulted in greater decrease in mangrove fraction in the southern region (Table 3.2).

Negative impacts attributed to the first MHW, Ningaloo Niño 10-11, was highest in the northern most and southern most regions (Figure 3.4), with total mangrove fraction decrease 3 times greater in the south region compared to the north region, and a larger area with high decrease detected in the south region (Table 3.2 and Figure 3.5). This trend of larger mangrove fraction decreases in the north and south is similar following the co-occurring Cyclone Carlos, but it is difficult to attribute these trends to this event when the comparable event, Ningaloo Niño 12-13 also displays this (Table 3.2 and Figure 3.5). Cyclone Quang and Ningaloo Niña 15-16 resulted in similar mangrove decrease across the study region, however, Quang resulted in greater high impact across all regions (Table 3.2 & Figure 3.5).

Increases in mangrove fraction as a consequence of the tropical cyclones were all higher in the northern regions, this was also generally true for the other climatic events (Table 3.2 & Figure 3.4). The drought and MHW events that co-occurred with a cyclone also resulted in higher mangrove fraction increases in the northern region. However, spatial patterns in the mangrove fraction increases associated with each co-occurring event appear to be spatially different. After Cyclone Carlos the mangroves increase appear to be more scattered and actually more prominent in the south (algae in the north), and for Ningaloo Niño 10-11 the mangrove fraction increases were highest where there was highest decrease in mangrove fraction following Carlos (Figure 3.4a, Figure B.1a, Figure B.1d). Similar disparities in mangrove fraction changes were found for co-occurring Ningaloo Niña 15-16 and Cyclone Quang where spatial patterns on increase also appear dissimilar (Figure B.4 and Figure B.5), where areas of greater increases following Cyclone Quang have occurred as greater decreases for Ningaloo Niña 15-16 (Figure B.4d and Figure B.5).

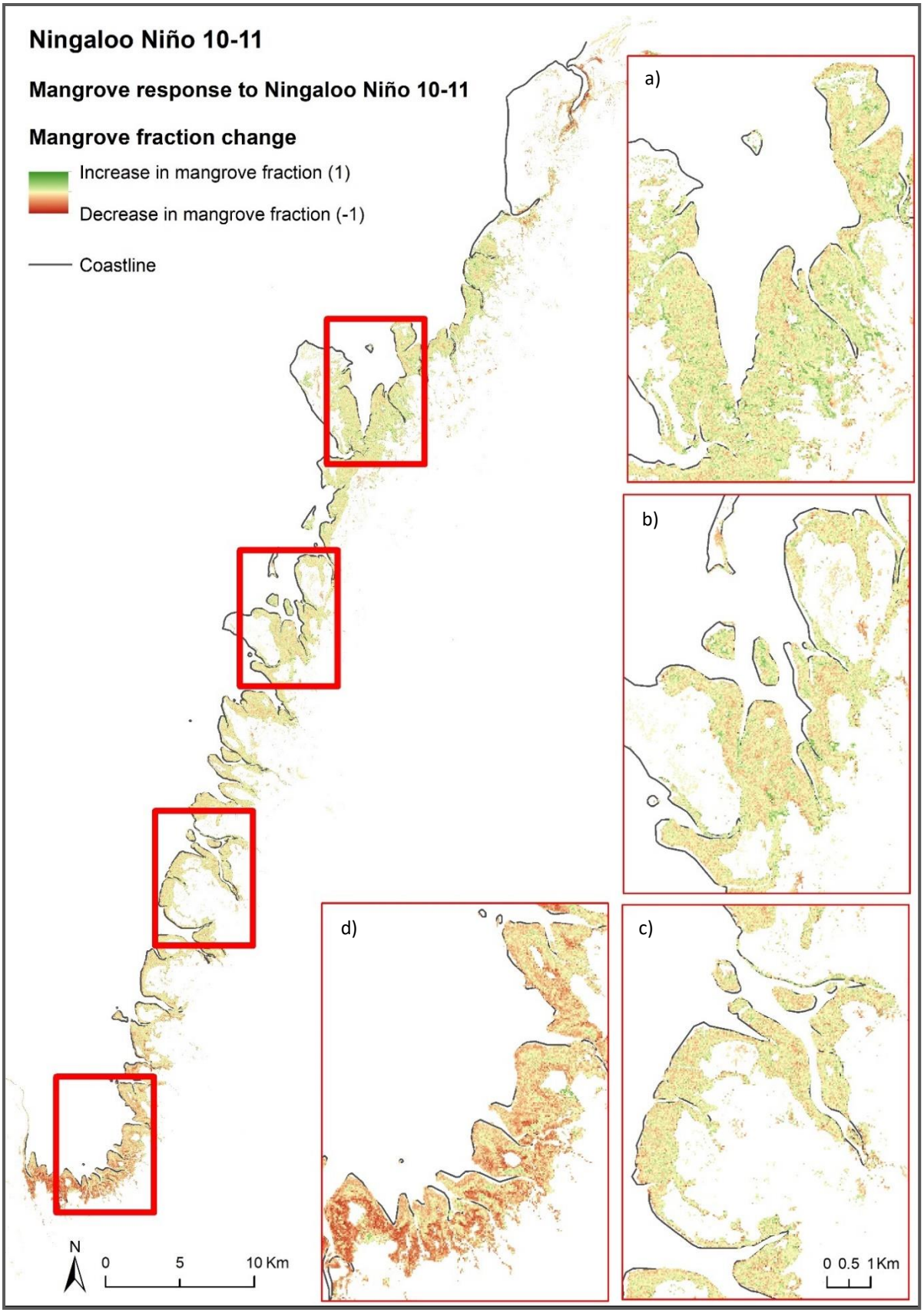


**Figure 3.4:** Mangrove fraction change map following Ningaloo Niño 10-11 where reds indicated mangrove fraction decreases and greens indicate mangrove fraction increases, including zoom insets of part of the northern (a), upper central (b), lower central (c), and southern localities of the study area. The scale of all insets is the same as in inset (c).

**Table 3.2:** Total proportion and area of decreases and increases in mangrove fraction across different regions of the study area, for each climatic event for the north (N), central (C) and south (S) regions, with the greatest total proportion of decreases and increases in mangrove for each region for each climatic event shaded grey. Decreases and increases are proportional to the pre-impact image date of mangroves for each region of the study area for each respective climatic event.

| | | Decreases | | Increases | |
|---|---|---|---|---|---|
| Climatic event / Region | | Proportion (%) | Area ($km^2$) | Proportion (%) | Area ($km^2$) |
| Cyclone Vance | N | 51.88 | 34.52 | 13.13 | 8.74 |
| | C | 56.58 | 23.69 | 5.37 | 2.25 |
| | S | 46.69 | 21.14 | 6.39 | 2.89 |
| Ningaloo Niña 02-03 | N | 41.30 | 17.08 | 2.76 | 1.14 |
| | C | 31.69 | 9.20 | 2.62 | 0.76 |
| | S | 31.90 | 11.60 | 3.86 | 1.40 |
| Ningaloo Niño 10-11 | N | 7.53 | 13.20 | 8.19 | 17.92 |
| | C | 4.32 | 8.65 | 4.71 | 6.95 |
| | S | 21.01 | 7.52 | 2.21 | 9.91 |
| Cyclone Carlos | N | 15.58 | 5.56 | 24.23 | 3.29 |
| | C | 8.84 | 2.15 | 16.34 | 1.73 |
| | S | 7.85 | 4.22 | 13.63 | 1.74 |
| Ningaloo Niño 12-13 | N | 8.47 | 5.79 | 5.02 | 4.56 |
| | C | 5.38 | 4.09 | 4.32 | 2.36 |
| | S | 7.72 | 7.46 | 3.19 | 2.49 |
| Cyclone Quang | N | 16.46 | 3.77 | 22.34 | 4.11 |
| | C | 17.60 | 1.47 | 14.14 | 1.60 |
| | S | 14.78 | 8.56 | 19.48 | 0.90 |
| Ningaloo Niña 15-16 | N | 11.49 | 9.88 | 9.04 | 15.36 |
| | C | 10.11 | 3.10 | 5.83 | 5.73 |
| | S | 17.19 | 3.23 | 5.74 | 5.61 |

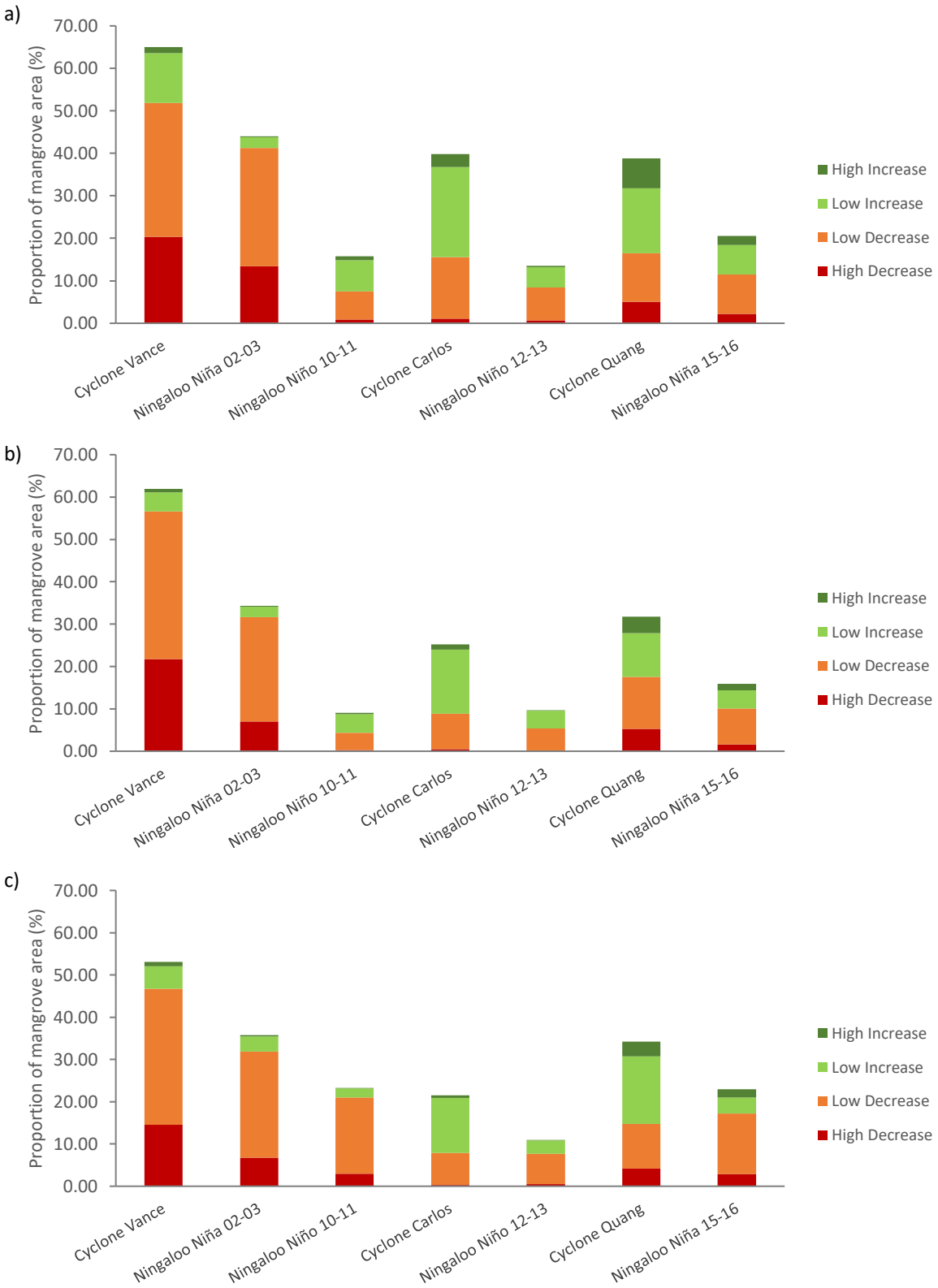


**Figure 3.5:** Proportion of mangrove area experiencing fraction increase and decrease per change class across the north (a), central (b), and south (c) regions of the study area for each climatic event in chronological order. Mangrove fraction change are proportional to the pre-impact image date of mangroves for the regions of the study area for each respective climatic event.

### 3.1.3 Impacts across different distances from the coastline

Negative mangrove response across different distances from the coastline to other and comparable climatic events here often exhibited opposite trends. The only comparable climatic events that had similar trend in negative impact across different distance from the coast were the MHWs, with increased negative impact on the distances closest and furthest from the coast, this was also the general pattern for Cyclone Vance and Quang, however, Cyclone Carlos resulted in greater mangrove decrease further away from the coastline (Table 3.3). The two drought events resulted in opposite responses from mangroves, with higher mangrove fraction decrease closest to the coast after Ningaloo Niña 02-03 and further from to the coast after Ningaloo Niña 15-16 (Table 3.3).

Decreases in mangrove fraction within 200m of the coastline are most prominent in the northern and central section of the study area following Cyclone Vance (Figure 3.1a,c), and most common at ~1000m from the coast following Cyclone Carlos in the north (Figure B.1a) and in the south following drought event, Ningaloo Niña 15-16 (Figure B.4d).

Mangrove fraction decrease after Cyclone Vance followed a different trend depending on the change class, where the proportional area of high decrease in mangrove fraction declined with increasing distance from the coast, and vice versa for low decrease in mangrove fraction (Figure 3.6a). The other climate events had high and low increasing and decreasing trends in mangrove fraction that followed general trend of their respective total decreases.

Increases in mangrove fraction were generally higher further from the coast for all climatic events, especially following Cyclone Carlos and Vance (Table 3.3). Cyclone Carlos resulted in a 42.2% increase in area mangrove fraction ~1000m from the coast, with low class mangrove fraction increase expanding rapidly in area, and high class increase more subtly, further from the coast (Table 3.3 and Figure 3.6d).

**Table 3.3:** Total proportion and area of decreases and increases in mangrove fraction across different distances from the coast at 200m intervals up to 1000m, with the greatest total proportion of decreases and increases in mangrove fraction across landward margins for each climatic event shaded grey. Decreases and increases are proportional to the pre-impact image date of mangroves for each distance from the coast of the study area for each respective climatic event

| | | Decreases | | Increases | |
|---|---|---|---|---|---|
| Climatic event | Distance from the coast | Proportion (%) | Area ($km^2$) | Proportion (%) | Area (km2) |
| Vance | 200m | 55.16 | 28.82 | 3.94 | 3.94 |
| | 400m | 46.08 | 13.92 | 7.96 | 7.96 |
| | 600m | 47.65 | 8.97 | 10.23 | 10.23 |
| | 800m | 51.59 | 6.54 | 11.20 | 11.20 |
| | 1000m | 53.57 | 4.97 | 10.03 | 10.03 |
| Ningaloo Niña 02-03 | 200m | 38.24 | 14.82 | 3.42 | 3.42 |
| | 400m | 39.48 | 10.57 | 2.46 | 2.46 |
| | 600m | 36.50 | 5.51 | 3.40 | 3.40 |
| | 800m | 31.19 | 2.58 | 3.90 | 3.90 |
| | 1000m | 29.20 | 1.37 | 3.49 | 3.49 |
| Ningaloo Niño 10-11 | 200m | 11.29 | 5.67 | 4.42 | 4.42 |
| | 400m | 10.84 | 3.40 | 5.05 | 5.05 |
| | 600m | 9.76 | 1.74 | 6.19 | 6.19 |
| | 800m | 9.24 | 0.95 | 6.56 | 6.56 |
| | 1000m | 11.09 | 0.64 | 6.70 | 6.70 |
| Carlos | 200m | 7.55 | 2.76 | 3.95 | 2.69 |
| | 400m | 8.68 | 0.98 | 7.26 | 3.31 |
| | 600m | 12.31 | 0.78 | 16.46 | 4.77 |
| | 800m | 13.71 | 0.73 | 26.45 | 5.65 |
| | 1000m | 15.44 | 0.64 | 42.20 | 8.12 |
| Ningaloo Niño 12-13 | 200m | 5.12 | 5.11 | 2.69 | 6.11 |
| | 400m | 2.94 | 3.44 | 3.31 | 5.07 |
| | 600m | 3.88 | 2.52 | 4.77 | 6.61 |
| | 800m | 5.82 | 1.78 | 5.65 | 9.69 |
| | 1000m | 8.17 | 1.19 | 8.12 | 11.16 |
| Quang | 200m | 11.29 | 5.67 | 4.42 | 4.42 |
| | 400m | 10.84 | 3.40 | 5.05 | 5.05 |
| | 600m | 9.76 | 1.74 | 6.19 | 6.19 |
| | 800m | 9.24 | 0.95 | 6.56 | 6.56 |
| | 1000m | 11.09 | 0.64 | 6.70 | 6.70 |
| Ningaloo Niña 15-16 | 200m | 10.18 | 3.63 | 6.11 | 3.95 |
| | 400m | 10.53 | 2.62 | 5.07 | 7.26 |
| | 600m | 13.17 | 2.15 | 6.61 | 16.46 |
| | 800m | 16.01 | 1.38 | 9.69 | 26.45 |
| | 1000m | 19.40 | 0.88 | 11.16 | 42.20 |

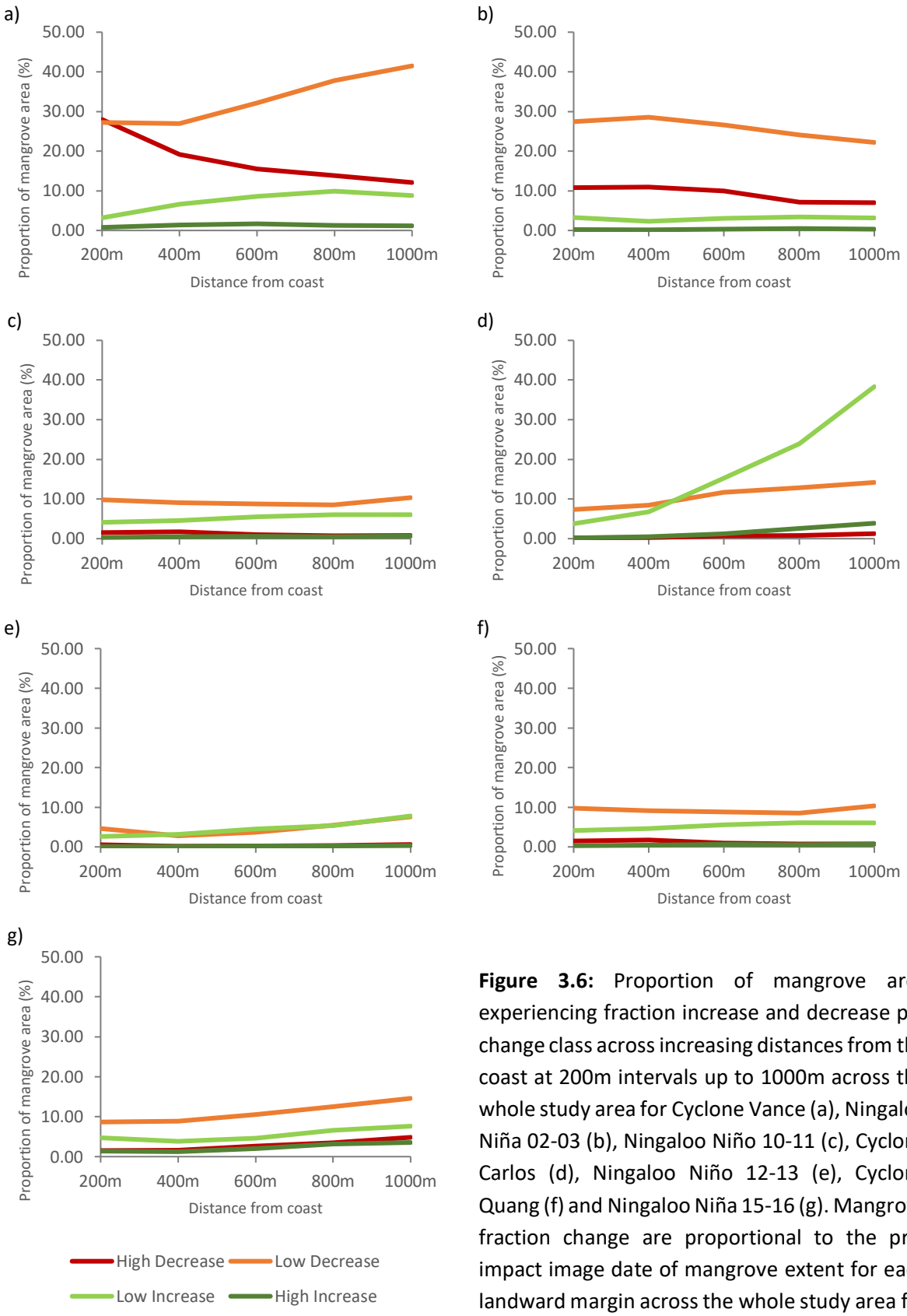


**Figure 3.6:** Proportion of mangrove area experiencing fraction increase and decrease per change class across increasing distances from the coast at 200m intervals up to 1000m across the whole study area for Cyclone Vance (a), Ningaloo Niña 02-03 (b), Ningaloo Niño 10-11 (c), Cyclone Carlos (d), Ningaloo Niño 12-13 (e), Cyclone Quang (f) and Ningaloo Niña 15-16 (g). Mangrove fraction change are proportional to the pre-impact image date of mangrove extent for each landward margin across the whole study area for each respective climatic event.

## 3.2 Recovery

This study tracked the recovery of mangroves from the extreme climatic events that occurred early enough to study for 10 years after the impact. Mangrove recovery trajectories were variable (Figure 3.7), with recovery following the different events here showing varying trends in recovery rates and variable recovery time (Figure 3.8 – Figure 3.13). Overall, only a small number of pixels in comparison to the mangrove extent that were impacted were found suitable to be modelled (Table 3.4), this could indicate more complex mechanisms of recovery than what could be modelled here in ten years after variable impacts, and cumulative impacts. On average, the initial trajectory of mangrove fraction across the study following any climatic impact was positive, indicating that on average mangroves are recovering however, these rates of recovery differed marginally per event (Table 3.4), with recovery rates following Cyclone Vance 1999 and the drought event, Ningaloo Niña 02-03, being quite low across the study area (Figure 3.8 and Figure 3.10). The slowest average rates of mangrove recovery were after Cyclone Vance with initial recovery of 17% in area per year (± 20%) in impacted pixels (Table 3.4) resulting in the longest average time to recover of 6.5 years (± 3 years). However, given the average modelling time of this initial recovery rate of 4 years, this calculated mangrove fraction trajectory is affected by the Ningaloo Niña 02-03. Ningaloo Niña 02-03 resulted in further decreases in mangrove fraction, potentially contributing to the slower rates of recovery, this can be seen marginally from Figure 3.13ii, where the second slope of recovery after Vance has been slowed by this event. The initial recovery rates following Ningaloo Niña 02-03 were higher at 21% in area per year (± 16%) and 5 years (± 3 years) on average to recover, and Ningaloo Niño 10-11 had on average the highest annual rates of recovery at 35% (± 23%) of impacted pixels resulting in the least time on average to recover of 2.5 years (± 2 years) (Table 3.4).

Ningaloo Niña 02-03, region-based recovery patterns did not show large variations in recovery rates or time to recover. After Cyclone Vance rates of recovery were slightly higher in the north and central region compared to the south, areas that were more negatively impacted after Vance (Table 3.4). Recovery times following both of these events were similar for the three regions (Table 3.4). This could be due to the different magnitude of the impact thus influencing recovery time. Additionally, the rates reported here are the initial phase of recovery where the second slope may differ between these two events, where recovery was

more likely found on the second slope, resulting in variable recovery time depending on annual rates of slope 2 (Figure 3.14a,b). Mangrove recovery rates following Ningaloo Niño 10-11 had variable rates and thus recovery time, where the north and south region exhibited higher initial rates of recovery and thus shorter time to recover (Table 3.4). These high annual rates of recovery for the north and south regions (38% ± 24% and 36% ± 23%, respectively) were the highest where mangroves had the greatest mangrove fraction decrease, in the northern most and southernmost extent with negligible recovery for other areas across the study area (Figure 3.11). The majority of this recovery in the northernmost and southern most extent of the study area appears to recover within a couple of years (Figure 3.12). Variability in recovery times across impacted regions after Ningaloo Niño 10-11 may be attributed to its shorter time frame of recovery, where many areas recovered within the initial slope of recovery (3.7c). In addition, there are pixels from all of these events with increasing initial recovery slopes potentially leading to recovery estimates that were subsequently followed by continued decrease (Figure 3.7ai,biii,ciii), where this following decreasing following recovery trends has not been captured by this study.

There was no clear trend across different distances from the coast with average mangrove recovery following Ningaloo Niña 02-03 and Ningaloo Niño 10-11, with fairly equal rates of recovery and years to recovery. However, average rates of mangrove recovery following Cyclone Vance did show a trend across distances from the coast where mangrove recovery tended to be slower initially and take longer to recover in areas closer to the coast to (Table 3.5, Figure 3.7, Figure 3.8). The annual rate of recovery within 200m of the coastline was 14% (± 18%) per year with a recovery time of 7 years (± 2.75 years) (Table 3.5). Higher magnitudes of mangrove impact closer to the coast also resulted in many areas along this margin not recovering in the observed time frame (Figure 3.9). Recovery rates and recovery time were up to two times faster ~800m from the coast following Cyclone Vance, then slightly slower on the furthest distance from the coast where a larger area of lower magnitude impact was recorded. Higher rates of recovery are mostly visible for around the northern and central regions further from the coast (Figure 3.8a,b and Figure 3.9a,b).

The drought event, Ningaloo Niña 02-03, did not appear to show any trends with the investigations here, exhibiting fairly moderate increases in mangrove fraction with patchy areas of slightly higher recovery rates scattered across mainly the northern and central

regions, with higher recovery rates seemingly in the northern region however on average this was not true (Figure 3.10 and Table 3.4). No trend was also found for the time frame for recovery with Figure 3.11 showing variable recovery times across regions and distances from coast; areas of no recovery within the observed time frame do however appear to be closer to the coast, however this was only slight. This would be similar to what was found with Cyclone Vance where areas of higher magnitude decrese had less recovery. However, unlike other events here, mangroves following Ningaloo Niña 02-03 did not exhibit higher rates of recovery in areas with larger areas of negative impact, or slower rates for areas that experienced higher magnitudes of impact.

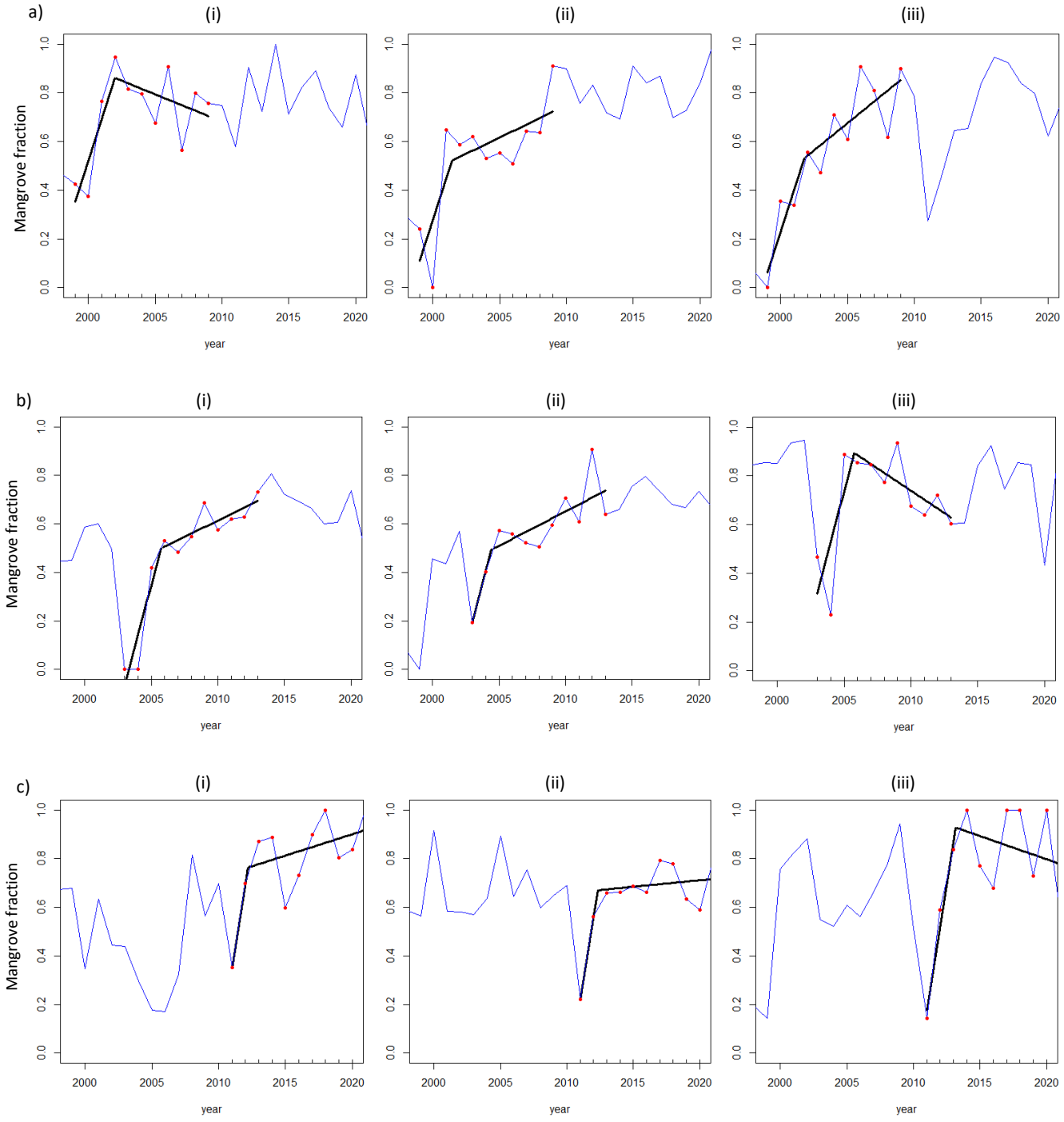


**Figure 3.7:** Mangrove fraction trajectories with initial recovery (slope 1) closest to average recovery for the whole study area per event as indicated in Table 3.4, after Cyclone Vance 1999 (a), Ningaloo Niña 02-03 (b), and Ningaloo Niño 10-11 (includes Cyclone Carlos) (c).


**Figure 3.8:** Initial slope of mangrove fraction trajectories following Cyclone Vance, where decreasing trajectories in mangrove fraction are indicated by red (i.e. further decrease) and increasing mangrove fraction trajectories are indicated by green (i.e. recovery), including zoom insets of part of the northern (a), upper central (b), lower central (c), and southern localities of the study area. The scale of all insets is the same as in inset (c).

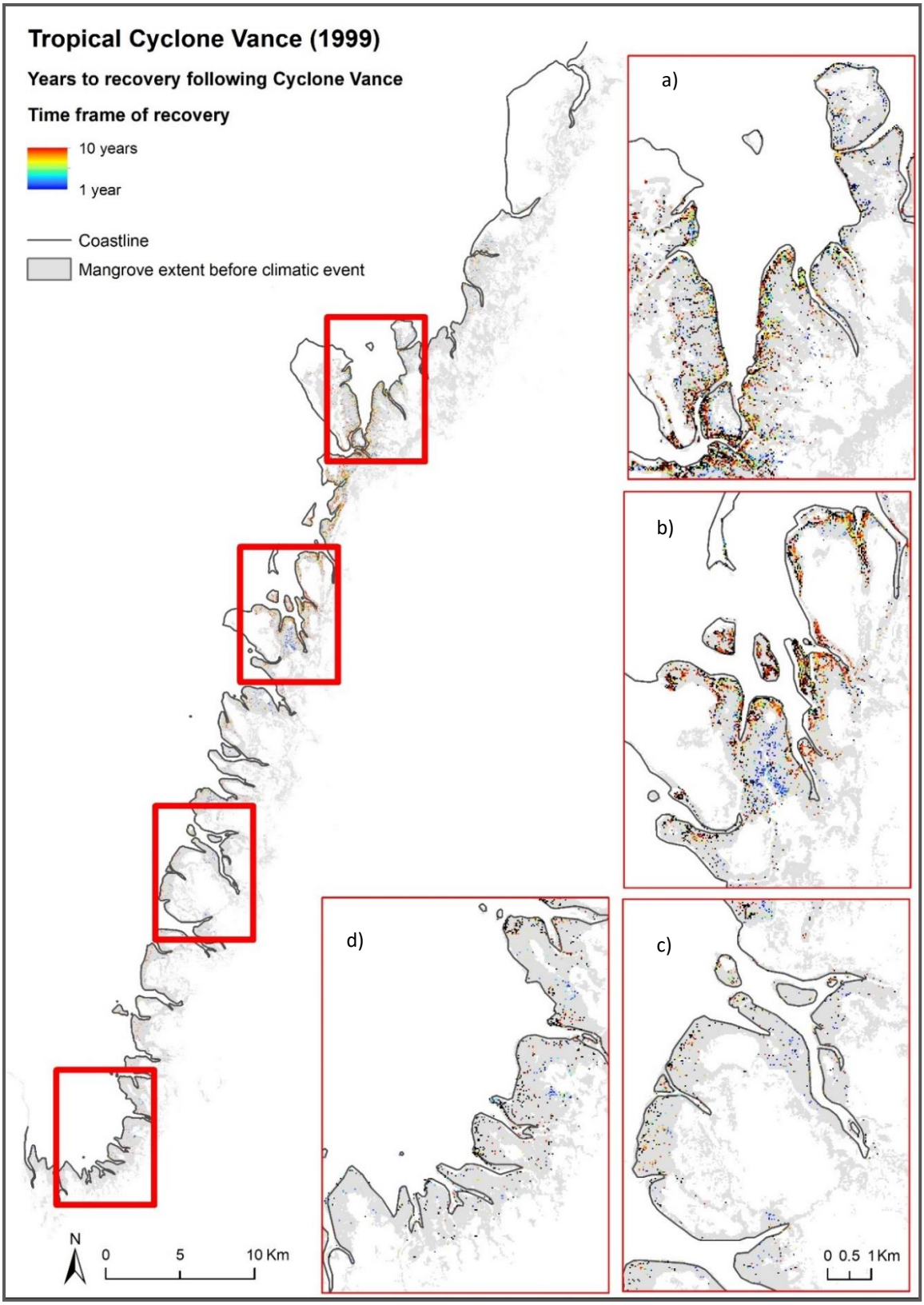


**Figure 3.9:** Time in years it took for mangrove fractions to reach pre-impact mangrove fractions (recovery time) following Cyclone Vance, where longer time frame of recovery is indicated by yellows and reds and a shorter time frame of recovery is indicated by light and dark blues, and no recovery in the observed time frame indicated by black, including zoom insets of part of the northern (a), upper central (b), lower central (c), and southern localities of the study area. The scale of all insets is the same as in inset (c).


**Figure 3.10:** Initial slope of mangrove fraction trajectories following Ningaloo Niña 02-03, where decreasing trajectories in mangrove fraction are indicated by red (i.e. further decrease) and increasing mangrove fraction trajectories are indicated by green (i.e. recovery), including zoom insets of part of the northern (a), upper central (b), lower central (c), and southern localities of the study area. The scale of all insets is the same as in inset (c).


**Figure 3.11:** Time in years it took for mangrove fractions to reach pre-impact mangrove fractions (recovery time) following Cyclone Vance, where longer time frame of recovery is indicated by yellows and reds and a shorter time frame of recovery is indicated by light and dark blues, and no recovery in the observed time frame indicated by black, including zoom insets of part of the northern (a), upper central (b), lower central (c), and southern localities of the study area. The scale of all insets is the same as in inset (c).

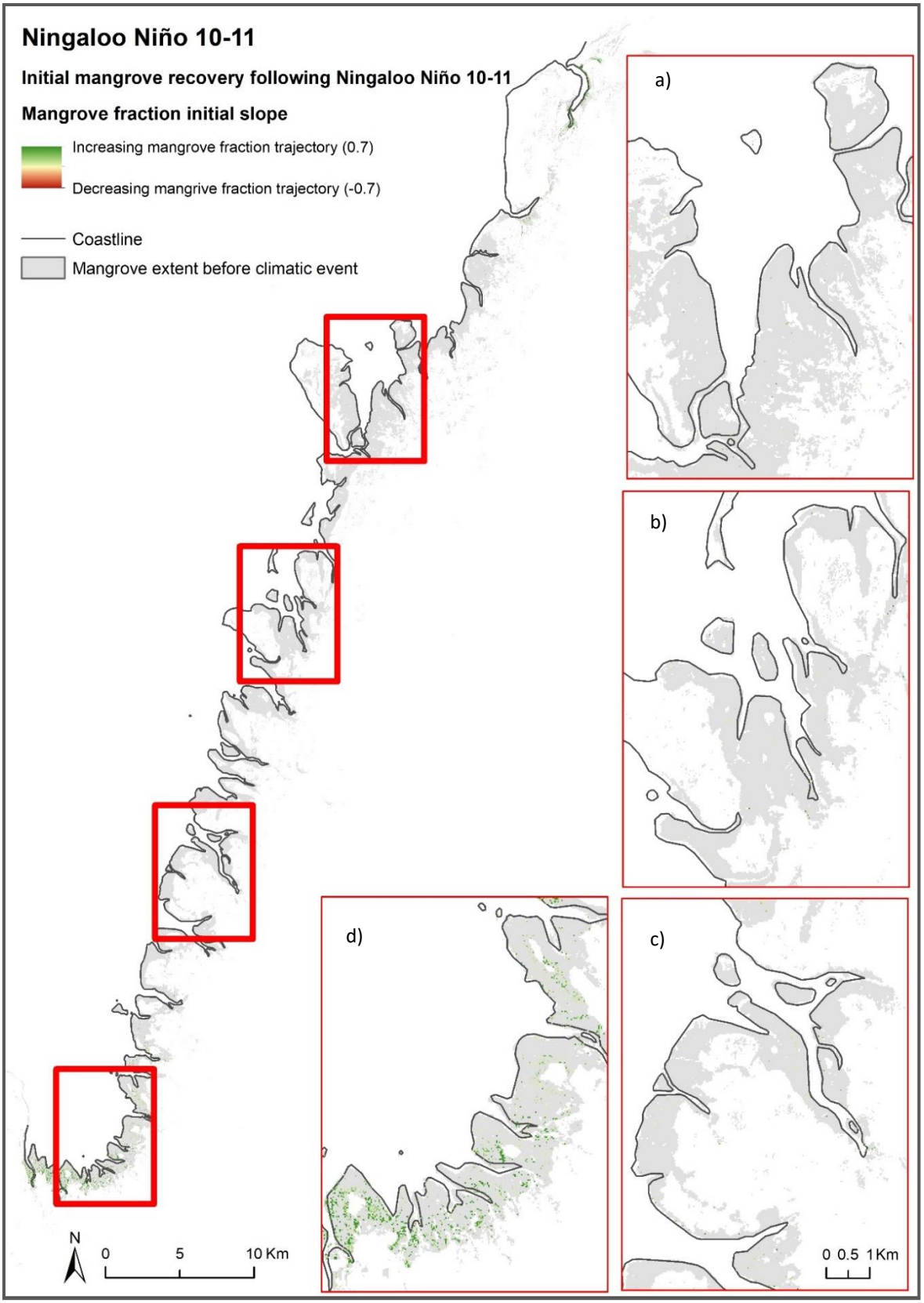


**Figure 3.12:** Initial slope of mangrove fraction trajectories following Ningaloo Niño 10-11, where decreasing trajectories in mangrove fraction are indicated by red (i.e. further decrease) and increasing mangrove fraction trajectories are indicated by green (i.e. recovery), including zoom insets of part of the northern (a), upper central (b), lower central (c), and southern localities of the study area. The scale of all insets is the same as in inset (c).

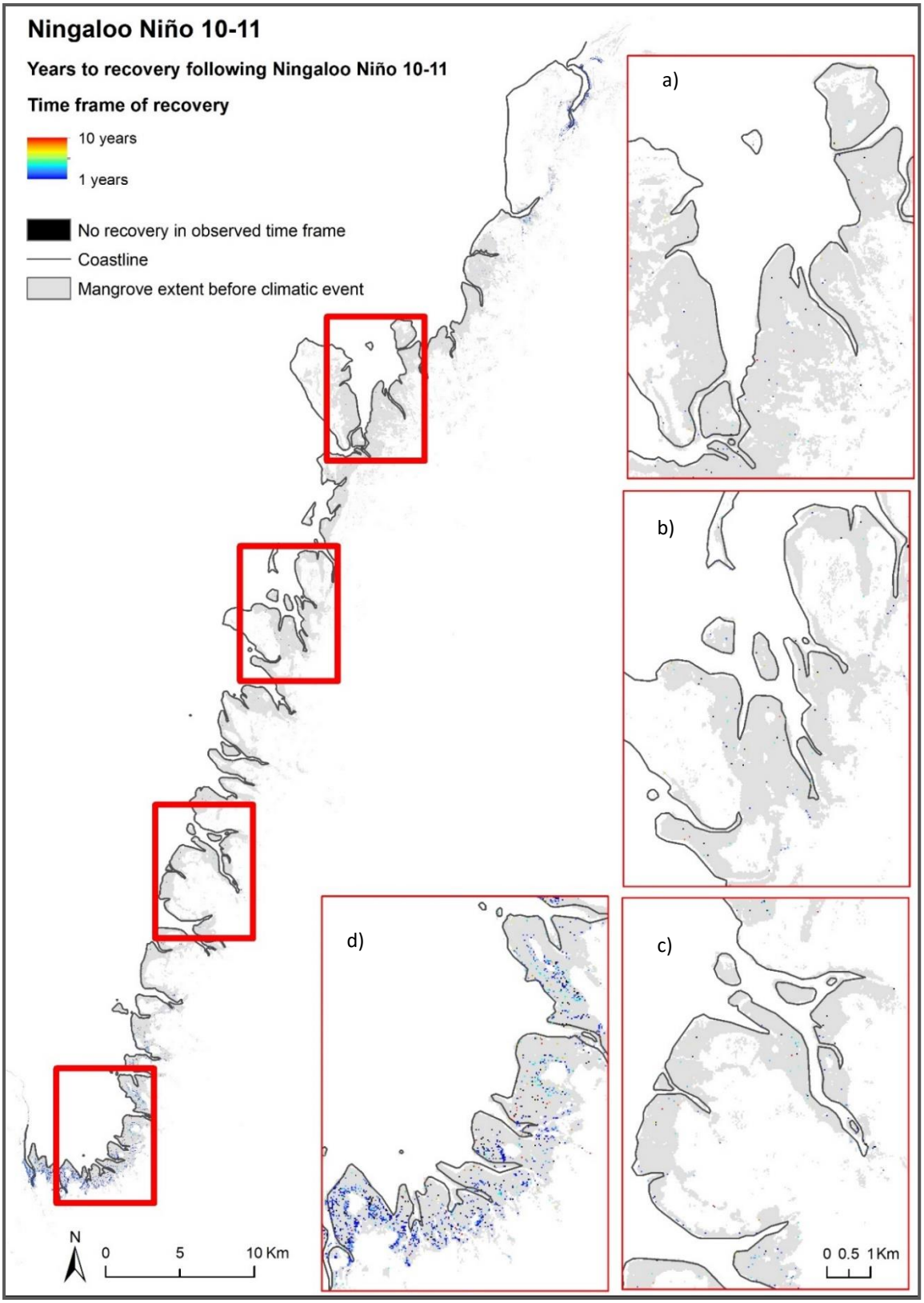


**Figure 3.13:** Time in years it took for mangrove fractions to reach pre-impact mangrove fractions (recovery time) following Ningaloo Niño 10-11, where longer time frame of recovery is indicated by yellows and reds and a shorter time frame of recovery is indicated by light and dark blues, and no recovery in the observed time frame indicated by black, including zoom insets of part of the northern (a), upper central (b), lower central (c), and southern localities of the study area. The scale of all insets is the same as in inset (c).

**Table 3.4:** Average (Mean) and standard deviation (SD) of recovery trajectories of mangrove fractions following each climatic event, where slope indicates the first slope and thus the initial trajectory of mangrove fraction (MF) and recovery time estimated over the 10 years of recovery for the whole study area (W), and the north (N), central (C) and south (S) regions of the study area where grey shading indicates the lowest rate of recovery and longest time to recover compared to all events for the whole study area and for each study area respective to each event.

| | | Initial recovery slope (MF/year) | | | Recovery time (years) | | | |
|---|---|---|---|---|---|---|---|---|
| Climatic event / Region | | Mean | SD | Mean slope years | Mean | SD | prop of area recovered* (%) | n suitable pixels modelled |
| Cyclone Vance | W | 0.17 | 0.20 | 4yrs (to 2003) | 6.55 | 3.02 | 53.9 | 16291 |
| | N | 0.19 | 0.20 | | 6.57 | 2.92 | | |
| | C | 0.16 | 0.21 | | 6.65 | 3.09 | | |
| | S | 0.12 | 0.21 | | 6.21 | 3.24 | | |
| Ningaloo Niña 02-03 | W | 0.21 | 0.16 | 3yrs (to 2006) | 5.04 | 2.57 | 72.0 | 22386 |
| | N | 0.21 | 0.17 | | 5.20 | 2.54 | | |
| | C | 0.20 | 0.16 | | 4.84 | 2.53 | | |
| | S | 0.21 | 0.15 | | 4.97 | 2.67 | | |
| Ningaloo Niño 10-11 | W | 0.35 | 0.23 | 2yrs (to 2013) | 2.61 | 1.95 | 85.2 | 3999 |
| | N | 0.38 | 0.24 | | 2.35 | 1.84 | | |
| | C | 0.15 | 0.16 | | 4.17 | 2.39 | | |
| | S | 0.36 | 0.23 | | 2.58 | 1.90 | | |

*Proportion of area recovered within 10 years

**Table 3.5:** Average (Mean) and standard deviation (SD) of recovery trajectories of mangrove fractions following each climatic event, where slope indicates the first slope and thus the initial trajectory of mangrove fraction (MF) and recovery time estimated over the 10 years of recovery across different distances from the coast (DC) over the whole study area, where grey shading indicates the lowest rate of recovery and longest time to recover for each climatic event.

| | | Slope (MF/year) | | Recovery time (years) | |
|---|---|---|---|---|---|
| Climatic event | DC | Mean | SD | Mean | SD |
| Cyclone Vance | 200m | 0.14 | 0.18 | 7.00 | 2.77 |
| | 400m | 0.17 | 0.22 | 6.50 | 3.06 |
| | 600m | 0.22 | 0.24 | 5.74 | 3.29 |
| | 800m | 0.28 | 0.25 | 4.80 | 3.26 |
| | 1000m | 0.26 | 0.25 | 5.46 | 3.37 |
| Ningaloo Niña 02-03 | 200m | 0.21 | 0.16 | 4.92 | 2.65 |
| | 400m | 0.20 | 0.16 | 5.10 | 2.57 |
| | 600m | 0.21 | 0.16 | 5.15 | 2.48 |
| | 800m | 0.21 | 0.16 | 5.09 | 2.47 |
| | 1000m | 0.20 | 0.16 | 5.05 | 2.46 |
| Ningaloo Niño 10-11 | 200m | 0.36 | 0.24 | 2.63 | 2.04 |
| | 400m | 0.35 | 0.22 | 2.48 | 1.75 |
| | 600m | 0.33 | 0.22 | 2.68 | 1.96 |
| | 800m | 0.30 | 0.21 | 2.77 | 2.14 |
| | 1000m | 0.31 | 0.24 | 2.56 | 1.83 |

# 4.0 Discussion

This study aimed to evaluate mangrove response to a number of extreme climatic events and track recovery from these events over a ten-year period using satellite remote sensing. The results have demonstrated that cyclone and drought events were more extreme in their associated impacts and resulted in slower recovery rates and times depending on the magnitude of impact. A passing cyclone also generally led to a higher area of mangrove fraction increase.

## 4.1 Mangrove response to climatic impacts

Cyclone impacts were studied at finer temporal scale than drought and MHW events. This is particularly concerning as cyclones were among the highest disturbances on mangroves. Category 5 Cyclone Vance (1999) resulted in the largest negative impact on mangroves, decreasing the proportion of mangroves in half of the mangrove extent in less than two months. The other cyclone events were associated with the other largest negative impacts. In addition, cyclone impacts resulted in higher magnitudes of decreases in mangroves.

Cyclones tended to cause larger areas of impact at further distances from the coast overall, and Cyclone Vance and Quang also resulted in high decreases in mangrove fraction on the coast. High magnitude decreases on the coast have been attributed to sediment deposition following Vance, due to the high storm surge depositing oceanic sediment (Paling et al., 2008). Although not documented, it is likely Cyclone Carlos and Quang would have produced some degree of storm surge (Krauss & Osland, 2020). Higher Impacts closer to the coast were also found in Florida after a hurricane however, this was reported as uprooting by wind not sediment deposition (McCoy et al., 1996). Large areas of mangrove decrease further from the coast could be due to the structure of the mangrove community. More sparse mangrove stands higher on the intertidal zone are potentially at higher risk of windthrow damage compared to a dense collective closer to the coastline (Krauss & Osland, 2020).

Remarkably, the southernmost extent of mangroves following Cyclone Vance remained largely unaffected which could be due to several factors. Vance travelled parallel to the western facing coast, where cyclones occurring in the southern hemisphere are suggested to be most damaging in the immediate left quadrant of the cyclone, where this zone potentially

did not impact the southern area (Krauss & Osland, 2020). However, it has been suggested by Paling et al., (2008) this was possibly due to inundation of small mangrove stands due to the storm surge. Mangroves in other areas have also been protected due to the storm surge from a cyclone occurring on a rising tide (Stocker, 1976).

Drought was also observed to have large negative impacts on mangroves. Drought events are associated with anomalously low sea level, little precipitation and anomalously high air temperatures which exacerbate dry and saline conditions that can exceed mangrove tolerances. Both long-term and El Niño associated drought has caused large scale mangrove die-back and mortality at both national and international scale (Barreto et al., 2008; Duke et al., 2017; Lovelock et al., 2017; Lucas et al., 2017; Otero et al., 2017; Paul et al., 2017; Servino et al., 2018; Asbridge et al., 2019). Large scale mangrove decline associated with drought is observed here via the same mechanisms with little rainfall, air temperatures 3 °C above average and anomalously low sea level. This drought event, Ningaloo Niña 02-03, occurred only three years after Cyclone Vance and resulted in the second largest negative impact in area and magnitude on mangroves, which further reduced mangroves in a third of their extent. This large-scale decline in Exmouth Gulf has previously gone unreported. This event resulted in higher mangrove decline, mainly in the north region of the study area and on the coastline, whereas Ningaloo Niña 15-16 resulted in higher decrease in the south and at further distance from the coast. The second drought event was associated with sea levels 30cm below average, which may have had greater influence on the southern region given the higher sea level variability in this area (AU Extreme Sea Levels (uwa.edu.au)), leading to higher salinities further from the coast.

Compound disturbances are most likely to intensify with climate change, delivering potentially more severe outcomes or potentially buffering mangroves from higher magnitude impacts. Tropical cyclones, when rain-bearing, can provide essential water input to arid mangrove ecosystems, to facilitate nutrients in these otherwise nutrient poor soils, which promotes the growth of mangroves (Lovelock et al., 2011; Adame et al., 2021). It is evident from the first drought event that negative impacts resulting from Ningaloo Niña 15-16 could have been more considerable if not for the co-occurring Cyclone Quang (2015). High rainfall associated with Cyclone Quang prior to this event may have provided an ecological buffer of

sorts, ameliorating drought associated with Ningaloo Niña 15-16. Ningaloo Niña 15-16 was associated with large impact in other regions of Australia (Duke et al., 2017; Lovelock et al., 2017; Asbridge et al., 2019). Cyclone Vance occurred after the peak of a strong El Niño phase that caused severely low sea level, and anomalously high air temperatures (no rainfall data available). Considering the similarities between this event and the Ningaloo Niña 02-03, some extent of mangrove decline could have been occurring prior to the storm. In addition, a second cyclone (category 2), Cyclone Steve (2000), passed nearby a year later (Black dotted line in Figure 1.1).

Further compound disturbances occurred in association with one marine heatwave (MHW), where the other, Ningaloo Niño 12-13 associated with higher SSTs did not result in much impact. Ningaloo Niño 10-11 was associated with mangrove decrease on the northernmost and southern most extent of the study area. Impact in the southern extent could be attributed to a reported locust outbreak in 2011. Reef et al., (2012) had discovered herbivory on *A. marina* in the southern region of eastern Exmouth Gulf. There has not been other documented herbivory of locusts on mangroves, however, given the remoteness of the region, this may not be surprising. Locust outbreaks are considered primarily climate related (Todd et al., 2002). Locust outbreaks in Africa have been linked to ENSO phases of climate variability, mostly La Niña (Todd et al., 2002). Mangrove decreases in the northernmost extent may be attributed to the co-occurring Cyclone Carlos (2011), as mangrove decrease following this event is in the same region. MHWs have not received much attention with associated impacts to mangroves. Anomalous warm SSTs in addition to hurricanes providing nutrients have been partly linked to mangrove expansion in Mexico during El Niño phases, however this was not recorded as a marine heatwave (López-Medellín et al., 2011).

Although cyclones were associated with some of the largest decreases, all cyclones also resulted in a larger area of increase in mangrove fraction and to a higher magnitude of increase compared to other events. Mangrove increases associated with extreme climatic events appear less reported. Increases in mangroves were higher in the north region and further landward following all climatic events. The Ningaloo Niño/Niña events that co-occurred with a cyclone had higher increase in the same regions as cyclones however these increases were spatially separate. These higher increases generally followed decreases identified from the event prior and vice versa.

## 4.2 Mangrove recovery from impacts

This study also aimed to track recovery from those events that resulted in negative impacts. It appears that areas that had the greatest proportion in area of mangrove fraction decline also exhibited greater initial rates of recovery. However, when a greater area underwent higher magnitudes of mangrove decrease, this resulted in significantly less recovery and thus longer recovery time. This trend was seen following Cyclone Vance where the mangroves closest to the coast that experienced higher degrees of loss resulted in slow initial recovery, with multiple areas in this zone not recovering. Lower magnitude impact following Vance led to greater recovery rates and less time to recover. However, this was not true for Ningaloo Niña 02-03, with areas of higher magnitudes of impact, and or greater areas of decline did not result in differences in initial recovery or recovery time, as trends in recovery were not observable in initial recovery. In contrast, negative impacts during the Ningaloo Niño 10-11 potentially due to Cyclone Carlos in the northernmost extent and locusts in the southernmost extent on mangroves, tended to recover within a few years. These impacts were associated with less area impacted overall and to lower magnitudes compared to Cyclone Vance and Ningaloo Niño 10-11, potentially meaning surrounding mangroves were in better condition to aid regeneration.

Slower recovery rates following Cyclone Vance could be attributed to the additional large-scale impact due to Ningaloo Niña 02-03, reducing the capacity of mangroves to recover from the first disturbance. Recovery time following both of these events exceeded previous estimates of recovery of 10 years (Paling et al., 2008), where areas here following both events exhibited areas still not recovered to pre-mangrove fractions at 10 years. This trend of compounding disturbances leading to slower recovery has been noted in Brazil, where drought followed an extreme hailstorm (Servino et al., 2018). In addition, recovery following drought events in general appear to be slow (Otero et al., 2017).

Recovery following these different events, cyclone, drought and MHW, could potentially mean that mangroves are initially at least, better at recovering from certain types of damage. Physical damage from wind and herbivory that resulted in moderate impact, even when over a large area, as seen on landward margin for Vance, and the southern and northern regions

for Ningaloo Niño 10-11, led to higher rates of recovery and recovery time. Longer lasting impacts disturbing environmental conditions such as sediment deposition and drought causing hypersaline soils, led to potentially slower mechanisms of recovery. Larger proportions of areas unaffected by the impact will serve as seed and propagule sources for impacted areas (Harris et al., 2018; Krauss & Osland, 2020), where areas with higher magnitudes of mangrove decline having fewer healthy surrounding mangroves to facilitate recovery compared to lower magnitude reductions. Many studies investigating recovery discuss species specific recovery mechanisms however this study has not achieved that level of investigation. Certain species and their assemblages are reported to be more sensitive to particular disturbances and have slower or faster regeneration rates (Paling et al., 2008; Asbridge 2015; Ayyappan et al., 2016; Villamayor et al., 2016; Asbridge et al., 2018; Krauss & Osland, 2020).

## 4.3 Limitations and future study

There were a few shortcomings in the approach used to detect and quantify impacts. This included some confusion between algal mats and mangrove land cover classes. Some of the high magnitude decreases and increase in mangrove fraction calculated following Cyclone Quang and Carlos were mostly in areas where algal mats dominate. This may indicate that there were not enough algal mat endmembers in the spectral library, as was the case with mangroves previously (see section 2.4.2.2) (see Li et al., 2005). In addition, considering miss modelling of algal mat, recovery rates could be influenced by opportunistic saltmarsh as documented by Paling et al., (2008) post-cyclone. Given time, these shortcomings could have been addressed.

It is likely that different species would have responded in different ways to different climatic events, and recover in different ways. However, species discrimination between mangroves is difficult to achieve with multispectral data especially considering the spatial resolution of 30m. Higher spatial and spectral resolutions may provide a better opportunity to investigate species specific mangrove response from different climatic events (Pham et al., 2019). However, this data type has limited archives making it difficult to investigate recovery, in

addition it can be costly to obtain. Other studies have used multiple vegetation indices to identify a time of year that species are spectrally distinct (Brewer et al., 2017).

Species level response and recovery in Exmouth Gulf would be particularly interesting for further study. Disturbances could be altering species compositions which could further influence types of recovery, and recovery time depending on the disturbance (Krauss & Osland, 2020). In addition, further studies should consider including the algal mat with investigations of impact and recovery as this also forms a major part of the ecosystem and may contribute to the recovery rates of mangroves. The long period of mangrove recovery could be attributed to a decline in active algal mat, where the algal mat provides much of the nutrients to mangroves and salt marsh during periods of rainfall (Humphreys et al. 2005). This contributes to understanding this ecosystem as a whole where studies on benthic coastal communities such as algal mats have received poor attention.

Mangrove ecosystems are constantly changing due partly to climatic events (Giri, 2016), with variations annually attributed to continued response and recovery of consecutive climatic impacts. Considering the small number of pixels able to model recovery, there could be more complex impact and recovery mechanisms happening that may take more years of data to understand. Five out of 10 years with a mangrove fraction may have been too stringent, not accounting for longer periods of mangrove mortality. In addition, compound impacts could be affecting mangrove recovery trajectory modelling leading to reduction in model fit (low adjusted R square). This study was however interested in the short-term recovery trajectories and initial recovery (slope 1), considering some of the more recent climatic events do not have enough data for short-term recovery let alone long-term recovery. Further studies should investigate the second slope of recovery, to determine if recovery was stable.

# 5.0 Conclusions

Cyclones are projected to become more rain-bearing and more extreme with global warming and climate change (Chang, 2017; Scoccimarro et al., 2017; Parker et al., 2018), with cyclones already increasing in severity and frequency since 1970 (Hartmann et at., 2013). Droughts are also expected to increase and anticipated to contribute substantially to mangrove decline,

especially in north west Australia (Alongi, 2015). In addition, extreme El Niño and La Niña events are also projected increase (Cai et al., 2014, Cai et al., 2015).

These projections are particularly concerning as, cyclones and drought events were associated with higher impact and slow recovery. In addition, higher rainfall associated with cyclones may help ameliorate drought, but may also cause flooding which disturbs sediment accretions. Further, cyclones may disturb coastal elevation through coastal erosion which may have implications on mangrove survival with projected sea level rise (Osland et al., 2020). There are many compound disturbances which have resulted in cumulative impacts leading to both positive and negative outcomes. It was demonstrated in this study that especially for cumulative impacts, mangroves may need more than ten years to fully recover from substantial disturbances, like Cyclone Vance and Ningaloo Niña 02-03, but especially when these impacts occur close in time. This could result in continued degradation of mangrove communities when not fully recovered. MHWs themselves did not appear associated with high negative impact, however MHWs are expected to increase in severity, frequency and duration (Cowan et al., 2014), where tolerances may one day be reached.

Some negative impacts on mangroves in Exmouth Gulf have largely gone unreported, potentially due to the remote region, which may not have been identified if not for remote sensing data. This indicates the need to monitor this important ecosystem more closely, and long term, especially given climate change posing a further challenge for mangrove survival.

# 6.0 References

Adame, M. F., Reef, R., Santini, N. S., Najera, E., Turschwell, M. P., Hayes, M. A., Masque, P., & Lovelock, C. E. (2021). Mangroves in arid regions: Ecology, threats, and opportunities. *Estuarine, Coastal and Shelf Science*, *248*, 106796.

Adams, J. B. (1993). Imaging spectroscopy: Interpretation based on spectral mixture analysis. *Remote geochemical analysis: Elemental and mineralogical composition*, 145-166.

Alongi, D. M. (2015). The impact of climate change on mangrove forests. *Current Climate Change Reports*, *1*(1), 30-39.

Asbridge, E, F., Lucas, R., Accad, A., & Dowling, R. (2015). Mangrove response to environmental changes predicted under varying climates: case studies from Australia. *Current Forestry Reports*, *1*(3), 178-194.

Asbridge, E., Lucas, R., Rogers, K., & Accad, A. (2018). The extent of mangrove change and potential for recovery following severe Tropical Cyclone Yasi, Hinchinbrook Island, Queensland, Australia. *Ecology and evolution*, *8*(21), 10416-10434.

Asbridge, E. F., Bartolo, R., Finlayson, C. M., Lucas, R. M., Rogers, K., & Woodroffe, C. D. (2019). Assessing the distribution and drivers of mangrove dieback in Kakadu National Park, northern Australia. *Estuarine, Coastal and Shelf Science*, *228*, 106353.

Australian Government. Bureau of Meteorology. (2012). Record-breaking La Niña events. Available at: http://www.bom.gov.au/climate/enso/history/La-Niña-2010-12.pdf.

Australian Government. Bureau of Meteorology. (2021). Climate Data Online. Available at: http://www.bom.gov.au/climate/data/index.shtml?bookmark=136&zoom=1&lat=-26.7905&lon=121.3165&layers=B00000TFFFFFFFTFFFFFFFFFFFFFFFFFFTTT&dp=IDC10002-d.

Australian Government. Bureau of Meteorology. (ND). *Monthly sea levels for Exmouth - 1989 to 2019*. Available at: http://www.bom.gov.au/ntc/IDO70000/IDO70000_62435_SLD.shtml.

Australian Government. Geoscience Australia. (2004). GEODATA COAST 100K 2004. Accessible at: https://data.gov.au/data/dataset/geodata-coast-100k-2004.

Ayyappan, N., Stephen, A., Muthusankar, G., Jeyakumar, S., & Presena, J. (2016). Spatio-temporal changes in fringe mangrove extent in Pondicherry, India after two phenomenal perturbations: tsunami and cyclone Thane. *Tropical Ecology*, *57*(2), 361-368.

Babcock, R. C., Bustamante, R. H., Fulton, E. A., Fulton, D. J., Haywood, M. D., Hobday, A. J., Kenyon, R., Matear, R. J., Plaganyi, E. E., Richardson, A. J. & Vanderklift, M. A. (2019). Severe continental-scale impacts of climate change are happening now: Extreme

climate events impact marine habitat forming communities along 45% of Australia's coast. *Frontiers in Marine Science*, *6*, 411.

Ball, M. C., & Farquhar, G. D. (1984). Photosynthetic and stomatal responses of two mangrove species, *Aegiceras corniculatum* and *Avicennia marina*, to long term salinity and humidity conditions. *Plant Physiology*, *74*(1), 1-6.

Barbier, E. B., Hacker, S. D., Kennedy, C., Koch, E. W., Stier, A. C., & Silliman, B. R. (2011). The value of estuarine and coastal ecosystem services. *Ecological monographs*, *81*(2), 169-193.

Barreto, M. B. (2008). Diagnostics about the state of mangroves in Venezuela: Case studies from the National Park Morrocoy and Wildlife Refuge Cuare. In *Mangroves and halophytes: restoration and utilisation* (pp. 51-64). Springer, Dordrecht.

Bergstrom, D. M., Wienecke, B. C., van den Hoff, J., Hughes, L., Lindenmayer, D. B., Ainsworth, T. D., Baker, C. M., Bland, L., Bowman, D. M. J. S., Brooks, S. T., Candadell, J. G., Constable, A. J., Dafforn, K. A., Depledge, M. H., Dickson, C. R., Duke, N. C., Helmstedt, K. J., Holz, A., Johnson, C. R., McGeoch, M. A., Melbourne-Thomas, J., Morgain, R., Nicholson, E., Prober, S. M., Raymond, B., Ritchie, E. G., Robinson, S. A., Ruthrof, K. X., Setterfield, S. A., Sgro, C. M., Stark, J. S., Tavers, T., Trebilco, R., Ward, D. F. L., Wardle, G. M., Williams, K. J., Zylstra, P. J., & Shaw, J. D. (2021). Combating ecosystem collapse from the tropics to the Antarctic. *Global change biology*, 00, 1-12.

Brewer, W. L., Lippitt, C. L., Lippitt, C. D., & Litvak, M. E. (2017). Assessing drought-induced change in a piñon-juniper woodland with Landsat: a multiple endmember spectral mixture analysis approach. *International Journal of Remote Sensing*, *38*(14), 4156-4176.

Cai, W., Borlace, S., Lengaigne, M., Van Rensch, P., Collins, M., Vecchi, G., Timmermann, A., Santoso, A., McPhaden, M. J., Wu, L., England, M. H., Wang, G., Guilyardi, E & Jin, F. F. (2014). Increasing frequency of extreme El Niño events due to greenhouse warming. *Nature climate change*, *4*(2), 111-116.

Cai, W., Wang, G., Santoso, A., McPhaden, M. J., Wu, L., Jin, F. F., Timmermann, A., Collins, M., Vecchi, G., Lengaigne, M., England, M. H., Dommenget, D., Takahashi, K., & Guilyardi, E. (2015). Increased frequency of extreme La Niña events under greenhouse warming. *Nature Climate Change*, *5*(2), 132-137.

Chang, E. K. (2017). Projected significant increase in the number of extreme extratropical cyclones in the Southern Hemisphere. *Journal of Climate*, *30*(13), 4915-4935.

Coupland, G. T., Paling, E. I., & McGuinness, K. A. (2005). Vegetative and reproductive phenologies of four mangrove species from northern Australia. *Australian Journal of Botany*, *53*(2), 109-117.

Cowan, T., Purich, A., Perkins, S., Pezza, A., Boschat, G., & Sadler, K. (2014). More frequent, longer, and hotter heat waves for Australia in the twenty-first century. *Journal of Climate*, *27*(15), 5851-5871.

CRAN. R. (2021). *Segmented: Regression Models with Break-Points/Change-Points Estimation*. Available at: https://cran.r-project.org/web/packages/segmented/index.html.

Dai, A. (2013). Increasing drought under global warming in observations and models. *Nature climate change*, *3*(1), 52-58.

Deepa, J. S., Gnanaseelan, C., Mohapatra, S., Chowdary, J. S., Karmakar, A., Kakatkar, R., & Parekh, A. (2019). The tropical Indian Ocean decadal sea level response to the Pacific decadal oscillation forcing. *Climate Dynamics*, *52*(7), 5045-5058.

de Jong, S. M., Shen, Y., de Vries, J., Bijnaar, G., van Maanen, B., Augustinus, P., & Verweij, P. (2021). Mapping mangrove dynamics and colonization patterns at the Suriname coast using historic satellite data and the LandTrendr algorithm. *International Journal of Applied Earth Observation and Geoinformation*, *97*, 102293.

Dennison, P. E., & Roberts, D. A. (2003). Endmember selection for multiple endmember spectral mixture analysis using endmember average RMSE. *Remote sensing of environment*, *87*(2-3), 123-135.

Dennison, P. E., Halligan, K. Q., & Roberts, D. A. (2004). A comparison of error metrics and constraints for multiple endmember spectral mixture analysis and spectral angle mapper. *Remote Sensing of Environment*, *93*(3), 359-367.

Duke, N. C. (1990). Phenological trends with latitude in the mangrove tree Avicennia marina. *The Journal of Ecology*, 113-133.

Duke, N. C., Kovacs, J. M., Griffiths, A. D., Preece, L., Hill, D. J., Van Oosterzee, P., Mackenzie, J., Morning, H. S., & Burrows, D. (2017). Large-scale dieback of mangroves in Australia's Gulf of Carpentaria: a severe ecosystem response, coincidental with an unusually extreme weather event. *Marine and Freshwater Research*, *68*(10), 1816-1829.

Feng, M., McPhaden, M. J., Xie, S. P., & Hafner, J. (2013). La Niña forces unprecedented Leeuwin Current warming in 2011. *Scientific reports*, *3*(1), 1-9.

Goldberg, L., Lagomasino, D., Thomas, N., & Fatoyinbo, T. (2020). Global declines in human-driven mangrove loss. *Global change biology*, *26*(10), 5844-5855.

Giri, C., Ochieng, E., Tieszen, L. L., Zhu, Z., Singh, A., Loveland, T., Masek, J., & Duke, N. (2011). Status and distribution of mangrove forests of the world using earth observation satellite data. *Global Ecology and Biogeography*, *20*(1), 154-159.

Giri, C. (2016). Observation and monitoring of mangrove forests using remote sensing: Opportunities and challenges. *Journal of remote sensing*, *8*(9), 783; https://doi.org/10.3390/rs8090783.

Gulf Holdings Pty. Ltd. (1990). Environmental Review and Management Programme: Onslaw Salt Project, Volume 1. Environmental Protection Authority (EPA) Archives. Available at: https://www.epa.wa.gov.au/sites/default/files/PER_documentation/A0164_R0495_ERMP_Volume%201.pdf.

Harris, R. M., Beaumont, L. J., Vance, T. R., Tozer, C. R., Remenyi, T. A., Perkins-Kirkpatrick, S. E., Mutchel, P. J., Nicotra, A. B., McGregor, S., Andrew, N. R., Letnic, M., Kearney, M. R., Wernberg, T., Hutley, L. B., Chambers, L. E., Fletcher, M. S., Keatley, M. R., Woodward, C. A., Williamson, G., Duke, N. C., & Bowman, D. M. J. S. (2018). Biological responses to the press and pulse of climate trends and extreme events. *Nature Climate Change*, *8*(7), 579-587.

Hartmann, D. L., Tank, A. M. K., Rusticucci, M., Alexander, L. V., Brönnimann, S., Charabi, Y. A. R., Dentener, F. J., Dlugokencky, E. J., Easterling, D. R., Kaplan, A., Soden, B. J., Thorne, P. W., Wild, M., & Zhai, P. (2013). Observations: atmosphere and surface. In *Climate change 2013 the physical science basis: Working group I contribution to the fifth assessment report of the intergovernmental panel on climate change* (pp. 159-254). Cambridge University Press.

He, M., Zhao, B., Ouyang, Z., Yan, Y., & Li, B. (2010). Linear spectral mixture analysis of Landsat TM data for monitoring invasive exotic plants in estuarine wetlands. *International Journal of Remote Sensing*, *31*(16), 4319-4333.

Hickey, S. M., Radford, B., Callow, J. N., Phinn, S. R., Duarte, C. M., & Lovelock, C. E. (2021). ENSO feedback drives variations in dieback at a marginal mangrove site. *Scientific reports*, *11*(1), 1-9.

Hobday, A. J., Alexander, L. V., Perkins, S. E., Smale, D. A., Straub, S. C., Oliver, E. C., Benthuysen, J. A., Burrows, M. T., Donat, M. G., Feng, M., Holdbrook, N. J., Moore, P. J., Scannell, H. A., Gupta, A. S., & Wernberg, T. (2016). A hierarchical approach to defining marine heatwaves. *Progress in Oceanography*, *141*, 227-238.

Humphreys, G., Paling, E. I., Craig, M., Kobryn, H., Sawers P., Eynon, H. (2005). Yannarie Salt Project Mangrove and Coastal Ecosystem Study: Baseline Ecological Assessment. Available at: https://www.epa.wa.gov.au/sites/default/files/PER_documentation/1295-ERMP-Appendix%204%20-%20Mangroves%20and%20Coast_Biota_CD.pdf.

Kataoka, T., Tozuka, T., Behera, S., & Yamagata, T. (2014). On the Ningaloo Niño/Niña. *Climate dynamics*, *43*(5-6), 1463-1482.

Kataoka, T., Masson, S., Izumo, T., Tozuka, T., & Yamagata, T. (2018). Can Ningaloo Niño/Niña Develop Without El Niño–Southern Oscillation?. *Geophysical Research Letters*, *45*(14), 7040-7048.

Krauss, K. W., & Osland, M. J. (2020). Tropical cyclones and the organization of mangrove forests: a review. *Annals of Botany*, *125*(2), 213-234.

Kruse, F. A., Lefkoff, A. B., Boardman, J. W., Heidebrecht, K. B., Shapiro, A. T., Barloon, P. J., & Goetz, A. F. H. (1993). The spectral image processing system (SIPS)—interactive visualization and analysis of imaging spectrometer data. *Remote sensing of environment*, *44*(2-3), 145-163.

Kuleshov, Y., Qi, L., Fawcett, R., & Jones, D. (2008). On tropical cyclone activity in the Southern Hemisphere: Trends and the ENSO connection. *Geophysical Research Letters*, *35*(14).

Lane, J., Jaensch, R., Lynch, R., & Elscot, S. (2001). A Directory of Important Wetlands in Australia: Western Australia. Chapter 12, 103 – 113. Available at: https://www.awe.gov.au/sites/default/files/documents/directory-ch12.pdf.

Li, L., Ustin, S. L., & Lay, M. (2005). Application of multiple endmember spectral mixture analysis (MESMA) to AVIRIS imagery for coastal salt marsh mapping: a case study in China Camp, CA, USA. *International Journal of Remote Sensing*, *26*(23), 5193-5207.

Loneragan, N. R., Adnan, N. A., Connolly, R. M., & Manson, F. J. (2005). Prawn landings and their relationship with the extent of mangroves and shallow waters in western peninsular Malaysia. *Estuarine, Coastal and Shelf Science*, *63*(1-2), 187-200.

López-Medellín, X., Ezcurra, E., González-Abraham, C., Hak, J., Santiago, L. S., & Sickman, J. O. (2011). Oceanographic anomalies and sea-level rise drive mangroves inland in the Pacific coast of Mexico. *Journal of Vegetation Science*, *22*(1), 143-151.

Lovelock, C. E., Feller, I. C., Adame, M. F., Reef, R., Penrose, H. M., Wei, L., & Ball, M. C. (2011). Intense storms and the delivery of materials that relieve nutrient limitations in mangroves of an arid zone estuary. *Functional Plant Biology*, *38*(6), 514-522.

Lovelock, C. E. (2008). Soil respiration and belowground carbon allocation in mangrove forests. *Ecosystems*, *11*(2), 342-354.

Lovelock, C. E., Feller, I. C., Reef, R., Hickey, S., & Ball, M. C. (2017). Mangrove dieback during fluctuating sea levels. *Scientific Reports*, *7*(1), 1-8.

Lucas, R., Finlayson, C. M., Bartolo, R., Rogers, K., Mitchell, A., Woodroffe, C. D., Asbridge, E, F., & Ens, E. (2017). Historical perspectives on the mangroves of Kakadu National Park. *Marine and Freshwater Research*, *69*(7), 1047-1063.

Lugo, A. E. (1997). Old-Growth Mangrove Forests in the United States: Bosques Maduros de Manglares en los Estados Unidos. *Conservation Biology*, *11*(1), 11-20.

Maggiorano, A., Feng, M., Wang, X. H., Ritchie, L., Stark, C., Colberg, F., & Greenwood, J. (2021). Hydrodynamic drivers of the 2013 marine heatwave on the North West Shelf of Australia. *Journal of Geophysical Research: Oceans*, *126*(3), e2020JC016495.

Markham, B. L., Storey, J. C., Williams, D. L., & Irons, J. R. (2004). Landsat sensor performance: history and current status. *IEEE transactions on geoscience and remote sensing*, *42*(12), 2691-2694.

Marshall, A. G., Hendon, H. H., Feng, M., & Schiller, A. (2015). Initiation and amplification of the Ningaloo Niño. *Climate dynamics*, *45*(9), 2367-2385.

May, S. M., Brill, D., Engel, M., Scheffers, A., Pint, A., Opitz, S., ... & Brückner, H. (2015). Traces of historical tropical cyclones and tsunamis in the Ashburton Delta (north-west Australia). *Sedimentology*, *62*(6), 1546-1572.

Maxar Technologies, Map data 2021. (2021). Available at: https://www.google.com/maps/@-22.0006699,114.4780213,38499m/data=!3m1!1e3.

McBride, J. L. (2012). The estimated cost of tropical cyclone impacts in Western Australia. In Technical Report. *Technical Report for the Indian Ocean Climate Initiative (IOCI) Stage 3*. Project 2.2.

McCreery, K., Orifici, R., Humphreys G. (2005). Yannarie Salt Project Flora and Vegetation Assessment: Baseline Botanical Survey. Available at: https://www.epa.wa.gov.au/sites/default/files/PER_documentation/1295-ERMP-Appendix%206%20-%20Flora%20and%20Veg_Biota.pdf.

McCoy, E. D., Mushinsky, H. R., Johnson, D., & Meshaka Jr, W. E. (1996). Mangrove damage caused by Hurricane Andrew on the southwestern coast of Florida. *Bulletin of Marine Science*, *59*(1), 1-8.

Merrifield, M. A., Thompson, P. R., & Lander, M. (2012). Multidecadal sea level anomalies and trends in the western tropical Pacific. *Geophysical Research Letters*, *39*(13).

Nagelkerken, I., Kleijnen, S., Klop, T., Van Den Brand, R. A. C. J., de La Moriniere, E. C., & Van der Velde, G. (2001). Dependence of Caribbean reef fishes on mangroves and seagrass beds as nursery habitats: a comparison of fish faunas between bays with and without mangroves/seagrass beds. *Marine Ecology Progress Series*, *214*, 225-235.

NASA. (2021). PO.DAAC: Sea surface temperature data. Available via link: LAS UI (nasa.gov).

NASA. (ND). PO.DAAC: GHRSST Level 4 MUR Global Foundation Sea Surface Temperature Analysis (v4.1). Available at: https://podaac.jpl.nasa.gov/dataset/MUR-JPL-L4-GLOB-v4.1.

Osland, M. J., Feher, L. C., Griffith, K. T., Cavanaugh, K. C., Enwright, N. M., Day, R. H., Stagg, C. L., Krauss, R. J., Grace, J. B., & Rogers, K. (2017). Climatic controls on the global distribution, abundance, and species richness of mangrove forests. *Ecological Monographs*, *87*(2), 341-359.

Osland, M. J., Feher, L. C., Anderson, G. H., Vervaeke, W. C., Krauss, K. W., Whelan, K. R., Balentine, K. M., Tiling-Range, G., Smith III, T. J., & Cahoon, D. R. (2020). A tropical cyclone-induced ecological regime shift: Mangrove forest conversion to mudflat in Everglades National Park (Florida, USA). *Wetlands*, *40*, 1445-1458.

Otero, X. L., Méndez, A., Nóbrega, G. N., Ferreira, T. O., Santiso-Taboada, M. J., Meléndez, W., & Macías, F. (2017). High fragility of the soil organic C pools in mangrove forests. *Marine pollution bulletin*, *119*(1), 460-464.

Paling, E. I., Kobryn, H. T., & Humphreys, G. (2008). Assessing the extent of mangrove change caused by Cyclone Vance in the eastern Exmouth Gulf, northwestern Australia. *Estuarine, Coastal and Shelf Science*, *77*(4), 603-613.

Parker, C. L., Bruyère, C. L., Mooney, P. A., & Lynch, A. H. (2018). The response of land-falling tropical cyclone characteristics to projected climate change in northeast Australia. *Climate dynamics*, *51*(9), 3467-3485.

Pastor-Guzman, J., Dash, J., & Atkinson, P. M. (2018). Remote sensing of mangrove forest phenology and its environmental drivers. *Remote sensing of environment*, *205*, 71-84.

Paul, A. K., Ray, R., Kamila, A., & Jana, S. (2017). Mangrove degradation in the Sundarbans. In *Coastal wetlands: alteration and remediation* (pp. 357-392). Springer, Cham.

Pham, T. D., Yokoya, N., Bui, D. T., Yoshino, K., & Friess, D. A. (2019). Remote sensing approaches for monitoring mangrove species, structure, and biomass: Opportunities and challenges. *Remote Sensing*, *11*(3), 230.

Powell, R. L., & Roberts, D. A. (2008). Characterizing variability of the urban physical environment for a suite of cities in Rondonia, Brazil. *Earth Interactions*, *12*(13), 1-32.

Reef, R., Ball, M. C., & Lovelock, C. E. (2012). The impact of a locust plague on mangroves of the arid Western Australia coast. *Journal of Tropical Ecology*, *28*(3), 307-311.

Roberts, D. A., Gardner, M., Church, R., Ustin, S., Scheer, G., & Green, R. O. (1998). Mapping chaparral in the Santa Monica Mountains using multiple endmember spectral mixture models. *Remote sensing of environment*, *65*(3), 267-279.

Roberts, D. A., Dennison, P. E., Gardner, M. E., Hetzel, Y., Ustin, S. L., & Lee, C. T. (2003). Evaluation of the potential of Hyperion for fire danger assessment by comparison to the Airborne Visible/Infrared Imaging Spectrometer. *IEEE Transactions on Geoscience and Remote Sensing*, *41*(6), 1297-1310.

Roth, L. C. (1992). Hurricanes and mangrove regeneration: effects of Hurricane Joan, October 1988, on the vegetation of Isla del Venado, Bluefields, Nicaragua. *Biotropica*, 375-384.

Scoccimarro, E., Villarini, G., Gualdi, S., Navarra, A., Vecchi, G., Walsh, K., & Zhao, M. (2017). Tropical cyclone rainfall changes in a warmer climate. In *Hurricanes and Climate Change* (pp. 243-255). Springer, Cham.

Servino, R. N., de Oliveira Gomes, L. E., & Bernardino, A. F. (2018). Extreme weather impacts on tropical mangrove forests in the Eastern Brazil Marine Ecoregion. *Science of the Total Environment*, *628*, 233-240.

Semeniuk, V. (1996). Coastal forms and Quaternary processes along the arid Pilbara coast of northwestern Australia. *Palaeogeography, Palaeoclimatology, Palaeoecology*, *123*(1-4), 49-84.

Sippo, J. Z., Lovelock, C. E., Santos, I. R., Sanders, C. J., & Maher, D. T. (2018). Mangrove mortality in a changing climate: An overview. *Estuarine, Coastal and Shelf Science*, *215*, 241-249.

Skilleter, G. A., Olds, A., Loneragan, N. R., & Zharikov, Y. (2005). The value of patches of intertidal seagrass to prawns depends on their proximity to mangroves. *Marine Biology*, *147*(2), 353-365.

Stocker, G. C. (1976). Report on cyclone damage to natural vegetation in the Darwin area after Cyclone Tracy 25 December 1974 [Northern Territory]. *Leaflet-Forestry and Timber Bureau (Australia).(no. 127).*

Sutton A.L. and Shaw J.L. (2021). Cumulative Pressures on the Distinctive Values of Exmouth Gulf. First draft report to the Department of Water and Environmental Regulation by the Western Australian Marine Science Institution, Perth, Western Australia. 272 pages.

Thayn, J. B. (2020). Monitoring Narrow Mangrove Stands in Baja California Sur, Mexico Using Linear Spectral Unmixing. *Marine Geodesy*, *43*(5), 493-508.

Todd, M. C., Washington, R., Cheke, R. A., & Kniveton, D. (2002). Brown locust outbreaks and climate variability in southern Africa. *Journal of Applied Ecology*, *39*(1), 31-42.

Unsworth, R. K., De León, P. S., Garrard, S. L., Jompa, J., Smith, D. J., & Bell, J. J. (2008). High connectivity of Indo-Pacific seagrass fish assemblages with mangrove and coral reef habitats. *Marine Ecology Progress Series*, 353, 213-224.

USGS. (ND). *Earth Explorer*. Available at: https://earthexplorer.usgs.gov/.

U.S. Geological Survey (USGS). (2021). Landsat 4-7: Collection 2 (C2) Level 2 Science Product (L2SP) Guide. LSDS-1618 Landsat 4-7 Collection 2 (C2) Level 2 Science Product (L2SP) Guide (amazonaws.com)

U.S. Geological Survey (USGS). (2021). Landsat 8: Collection 2 (C2) Level 2 Science Product (L2SP) Guide. Accessible at: LSDS-1619 Landsat 8 Collection 2 (C2) Level 2 Science Product (L2SP) Guide (amazonaws.com).

Villamayor, B. M. R., Rollon, R. N., Samson, M. S., Albano, G. M. G., & Primavera, J. H. (2016). Impact of Haiyan on Philippine mangroves: Implications to the fate of the widespread monospecific Rhizophora plantations against strong typhoons. *Ocean & Coastal Management*, *132*, 1-14.

Wang, J. J., Zhang, Y., & Bussink, C. (2014). Unsupervised multiple endmember spectral mixture analysis-based detection of opium poppy fields from an EO-1 Hyperion image in Helmand, Afghanistan. *Science of the Total Environment*, *476*, 1-6.

Western Australian Government. Environmental Protection Authority (EPA). (2009). Annual Report 2008 – 2009. Available at: https://www.epa.wa.gov.au/sites/default/files/Annual_reports/EPA-AR08-09.pdf.

Wilson, B. (2013). *The biogeography of the Australian North West Shelf: Environmental change and life's response*. Newnes.

Zhang, L., Han, W., Li, Y., & Shinoda, T. (2018). Mechanisms for generation and development of the Ningaloo Niño. *Journal of Climate*, *31*(22), 9239-9259.

# Appendix A

Landsat data image dates

**Table A.1:** Impact Data Images (Note: 2003 is the start of the scan line corrector error for Landsat 7, thus 2 image dates used for these years). Sea level (SL) time around 10am and 11am to see if sea kevel is rising.

| Event | Pre/Post | Satellite | Year | Date | SL 10 am (mm) | SL 11 am (mm) |
|---|---|---|---|---|---|---|
| Cyclone Vance | Pre | Landsat 5 | 1999 | 22-01-1999 | -14 | 212 |
| | Post | | | 04-04-1999 | 569 | 709 |
| Ningaloo Niña 02-03 | Pre | Landsat 7 | 2002 | 01-07-2002 | 127 | 238 |
| | Post | | 2003 | 05-08-2003 | -371 | -241 |
| | | | | 21-08-2003 | -285 | -274 |
| Ningaloo Niño 10-11 | Pre | Landsat 7 | 2010 | 07-07-2010 | 50 | -33 |
| | | | | 23-07-2010 | 273 | 95 |
| | Post | | 2011 | 11-08-2011 | 302 | 128 |
| | | | | 27-08-2011 | 323 | 183 |
| Ningaloo Niño 12-13 | Pre | Landsat 7 | 2012 | 12-07-2012 | -103 | -88 |
| | | | | 28-07-2012 | -237 | -285 |
| | Post | | 2013 | 31-07-2013 | -169 | -166 |
| | | | | 01-09-2013 | -13 | -105 |
| Cyclone Carlos | Pre | Landsat 7 | 2011 | 15-01-2011 | 69 | 127 |
| | | | | 31-01-2011 | 216 | 211 |
| | Post | | | 20-03-2011 | 636 | 621 |
| | | | | 05-03-2011 | 549 | 597 |
| Ningaloo Niña 15-16 | Pre | Landsat 8 | 2015 | 29-07-2015 | 195 | 28 |
| | Post | | 2016 | 31-07-2016 | 237 | 38 |
| Cyclone Quang | Pre | Landsat 8 | 2015 | 24-04-2015 | 339 | 519 |
| | Post | | | 10-05-2015 | 217 | 388 |

**Table A.2:** Recovery (days since rainfall recorded at Learmonth Airport)

| Satellite | Year | Date | Days Since Rain |
|---|---|---|---|
| Landsat 7 | 1999 | 9 July | 2 |
| Landsat 7 | 2000 | 12 August | 5 |
| Landsat 7 | 2001 | 31 August | 31 |
| Landsat 7 | 2002 | 1 July | 16 |
| Landsat 5 | 2003 | 12 July | 12 |
| Landsat 5 | 2004 | 15 August | 15 |
| Landsat 5 | 2005 | 1 July | 1 |
| Landsat 5 | 2006 | 4 July | 28 |
| Landsat 5 | 2007 | 8 August | 10 |
| Landsat 7 | 2008 | 17 July | 19 |
| | | 2 August | 1 |
| Landsat 7 | 2009 | 5 August | 15 |
| | | 21 August | 0 - 0.2 on this day – 11 since last |
| Landsat 7 | 2010 | 7 July | 20 |
| | | 23 July | 36 |
| Landsat 7 | 2011 | 11 August | 24 |
| | | 27 August | 5 |
| Landsat 7 | 2012 | 12 July | 1 |
| | | 28 July | 5 |
| Landsat 8 | 2013 | 8 August | 11 |
| Landsat 8 | 2014 | 10 July | 17 |
| Landsat 8 | 2015 | 29 July | 3 |
| Landsat 8 | 2016 | 31 July | 0 – 0.1 on this day – 6 since last |
| Landsat 8 | 2017 | 2 July | 17 |
| Landsat 8 | 2018 | 21 July | 9 – not quality controlled |
| Landsat 8 | 2019 | 9 August | 2 – not quality controlled |
| Landsat 8 | 2020 | 26 July | 8 – not quality controlled |

# Appendix B


**Figure B.1:** Mangrove fraction change map following Tropical Cyclone Carlos indicating mangrove fraction decreases (reds) and mangrove fraction increases (greens), including zoom insets of part of the northern (a), upper central (b), lower central (c), and southern localities of the study area. The scale of all insets is the same as in inset (c).

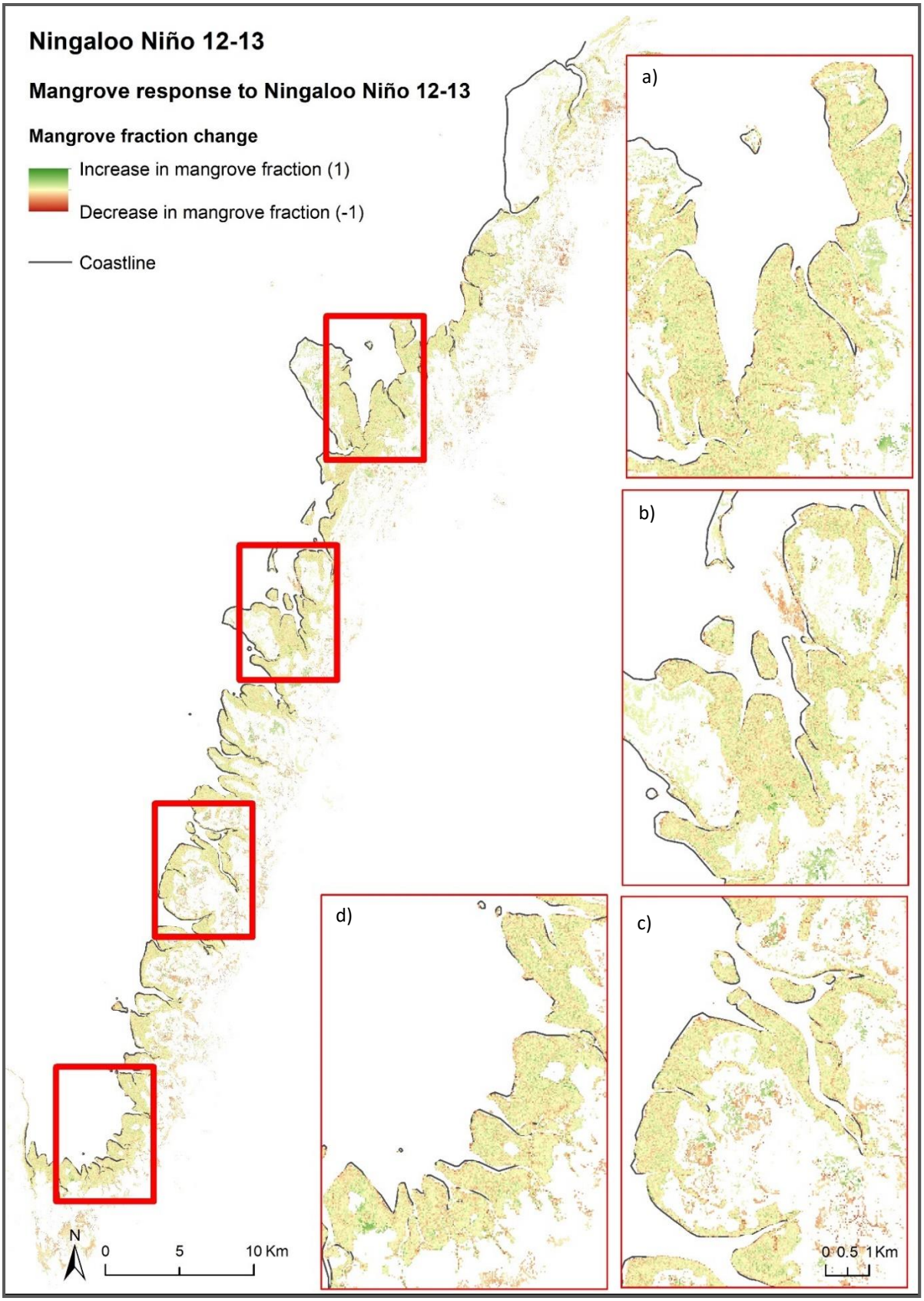


**Figure B.2:** Mangrove fraction change map following Tropical Cyclone Carlos where reds indicated mangrove fraction decreases and greens indicate mangrove fraction increases, including zoom insets of part of the northern (a), upper central (b), lower central (c), and southern localities of the study area. The scale of all insets is the same as in inset (c).

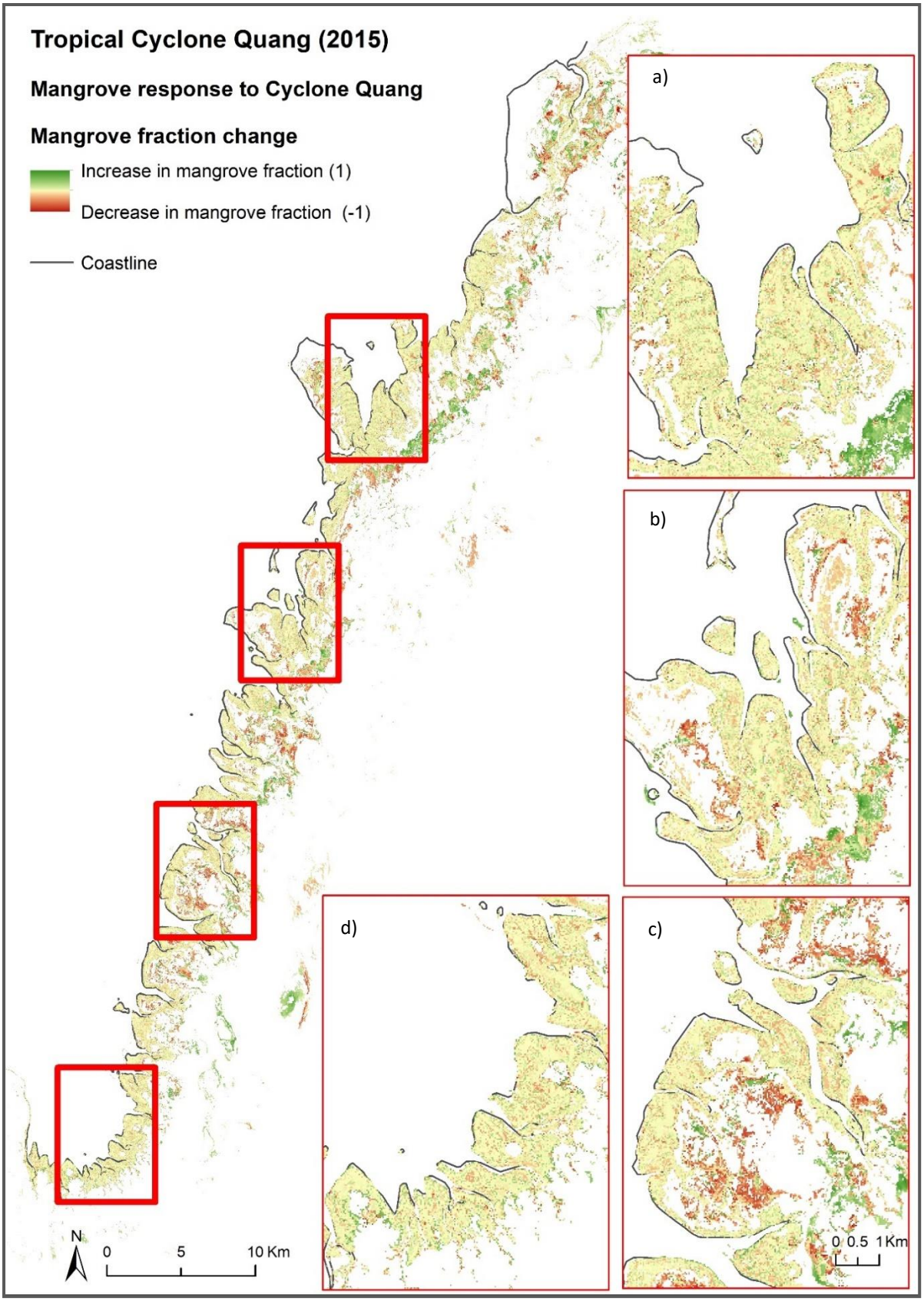


**Figure B.3:** Mangrove fraction change map following Tropical Cyclone Quang where reds indicated mangrove fraction decreases and greens indicate mangrove fraction increases, including zoom insets of part of the northern (a), upper central (b), lower central (c), and southern localities of the study area. The scale of all insets is the same as in inset (c).

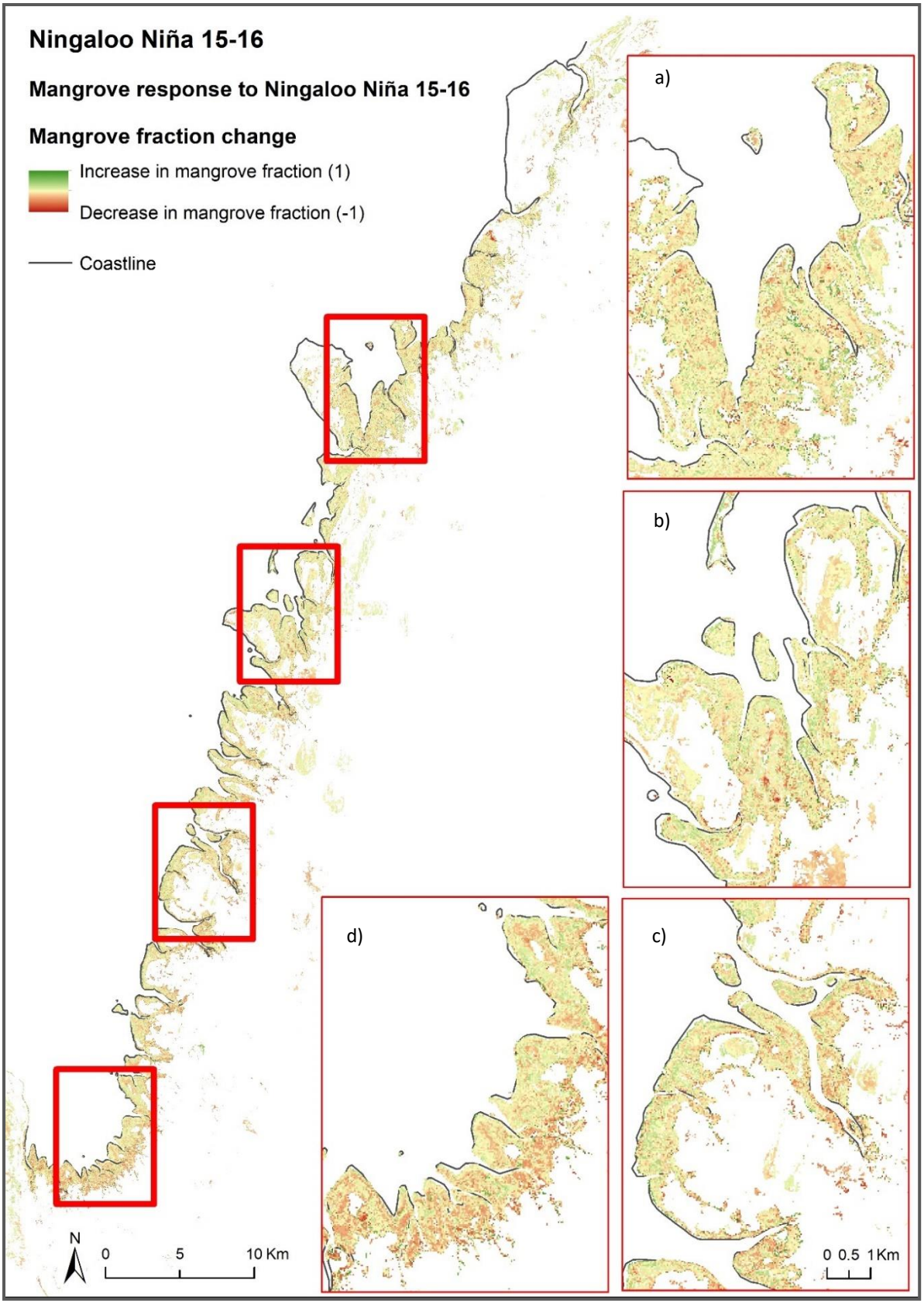


**Figure B.4:** Mangrove fraction change map following Ningaloo Niña 15-16 where reds indicated mangrove fraction decreases and greens indicate mangrove fraction increases, including zoom insets of part of the northern (a), upper central (b), lower central (c), and southern localities of the study area. The scale of all insets is the same as in inset (c).